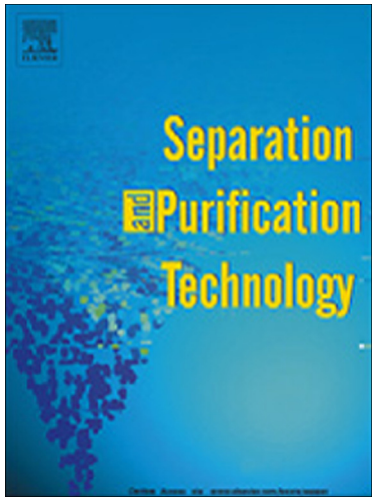

Modeling and Simulation Pressure–Temperature Swing Adsorption Process to Remove Mercaptan from Humid Natural Gas; A Commercial Case Study

Omid Taheri Qazvini, Shohreh Fatemi

PII: S1383-5866(14)00587-5
DOI: http://dx.doi.org/10.1016/j.seppur.2014.09.031
Reference: SEPPUR 11992

To appear in: *Separation and Purification Technology*

Received Date: 26 May 2014
Revised Date: 31 August 2014
Accepted Date: 30 September 2014

Please cite this article as: O.T. Qazvini, S. Fatemi, Modeling and Simulation Pressure–Temperature Swing Adsorption Process to Remove Mercaptan from Humid Natural Gas; A Commercial Case Study, *Separation and Purification Technology* (2014), doi: http://dx.doi.org/10.1016/j.seppur.2014.09.031

Modeling and Simulation Pressure–Temperature Swing Adsorption Process to Remove Mercaptan from Humid Natural Gas; A Commercial Case Study

Omid Taheri Qazvini and Shohreh Fatemi*

School of Chemical Engineering, Faculty of Engineering, University of Tehran, Tehran, Iran

ABSTRACT

Simulation of Pressure-Temperature Swing Adsorption (PTSA) process was performed in a commercial two-layer six-bed adsorption system during six sequential steps of cyclic operation to remove mercaptans from natural gas. The feed is a mixture of methane with water vapor, carbon dioxide, heavy hydrocarbons (C3+) and mercaptan impurities. The process is working in the cyclic operational mode to continuously reduce the mercaptan content from 134 to less than 10 ppmv which is determined as the standard level in the environmental regulations. The bed consists of two layers of activated alumina to specifically remove water vapor and 13X zeolite to remove mercaptan, respectively, from natural gas. The cycle steps i.e. adsorption at high pressure, depressurization to the lower pressure, two steps heating with purging hot purified natural gas, cooling the column and pressurization by feed were simulated sequentially. The dynamic model equations were constructed from four mole balances; model molecule of mercaptans, model molecule of heavy hydrocarbons, carbon dioxide and water vapor in natural gas, a total mass balance, a pressure drop equation and two energy balances of solid and gas phases in the adiabatic column. It was observed that the cyclic adsorption was approached to the steady conditions after seven cycles running the program. The predicted molar fractions out of the process were compared with the real results and good agreement was observed between the real data and simulated results. The influential parameters of the process were investigated through a parametric analysis of the process efficiency. Pressure of adsorption stage, purge to feed ratio at regeneration step and temperature of the 1st and 2nd heating steps were found to be the most influential parameters affecting the natural gas purification efficiency. For the sake of energy saving some suggestions were proposed for upgrading the design conditions with no significant effect on the purification performance. The results revealed that reduction of adsorption pressure from 6.8 to 6.1 Mpa, changing purge/feed ratio from 0.06 to 0.045, and combination two heating stages to one stage with 510 K and 12 h operation could be replaced in the operational conditions without significant changes in purification of the product.

Keywords: Cyclic adsorption process, PTSA commercial process, Mercaptan removal, natural gas purification, simulation

1. INTRODUCTION

Natural gas is a hydrocarbon gas mixture consisting primarily of methane including impurities of water vapor, carbon dioxide, sulfuric compounds such as hydrogen sulfide and light mercaptans (mostly ethyl and methyl mercaptan). Water and sulfur impurities cause several problems like corrosion, condensation, air pollution and lowering natural gas energy content. In the near future the environmental rule will force a reduction of sulfuric emission in the atmosphere (less than 20 molar ppmv) [1-3]. In the typical industrial plants, natural gas is separated from hydrogen sulfide by soda washing followed by amine-wash to separate other sulfuric compounds, and finally it is dried in the glycol dehydration unit. However, these treatments are not sufficient to completely separate sulfuric compounds and the presence of some light mercaptans would cause violation from environmental regulations [3]. As a result it would be necessary to add a new downstream treatment process to reduce sulfur down to the environmental issue requirements. In this situation, adsorption process as a simple, high selective and modern method that is developing for purification of natural gas would be an alternative process for sulfur removal.

A large number of modeling and simulation of gas cyclic adsorption are available in the literature. Kim et al. [4] investigated a parametric study on a six-step pressure swing adsorption (PSA) purifier using carbon molecular sieve to produce O_2 with a high purity. Knaebel et al. [5] simulated and optimized a pressure swing adsorption for recovering hydrogen from methane**.** Silva et al. [6] and Mendes et al. [7] studied the effect of operating parameters on separation of various mixtures after running a pressure swing adsorption process. Experimental studies on adsorption of various gases are countless but fundamental studies on the adsorption of mercaptans in the nanoporous materials are rarely found. Weber et al. [2] and Bellat et al. [3] measured adsorption equilibrium of binary ethyl mercaptan/hydrocarbon mixtures on a 13X zeolite. Bashkova et al. [8] also they presented adsorption equilibrium of methyl mercaptan on activated carbon adsorbent. In addition, there is much less reports about the cyclic adsorption processes for adsorption of mercaptan from natural gas. Shirani et al. [9] studied water vapor and mercaptan adsorption on 13X zeolite in natural gas purification process. Li Zhou et al .[10] studied removing of H_2S from natural gas by applying a pressure swing adsorption to investigate the possibility of purification.

For the case of deep desulfurization of natural gas, two main technologies (temperature swing adsorption (TSA) and pressure swing adsorption (PSA)) should be combined together. Pressure is required for the adsorption step and increasing temperature is required for the efficient regeneration of adsorbents in desorption step. Although the process of PTSA for natural gas purification from sulfur compounds was not found in the

literature survey, some studies are found for separation and purification by this process. Wan-Seon and et al. [11] proposed PTSA cyclic process for removing greenhouse gas SF_6 from a mixture of N_2 and 1.3% of SF_6 by activated carbon. The maximum purity of 19.5% and recovery of 50.1% were obtained with adsorption pressure of 2.5 atm, desorption temperature of 200 C and evacuation of 1 hour. Mulgundmath et al. [12] optimized a PTSA cyclic adsorption process for capturing carbon dioxide released from post combusted natural gas. In the study, Pressure Swing Adsorption (PSA) process has been compared with Thermal Pressure Swing Adsorption (TPSA) process for CO_2 recovery from a flue gas composition of 10% CO_2 (by vol) in N_2using Ceca 13X adsorbent. In another work, Pugsley et al. [13] simulated a novel CO_2 separation process known as the circulating fluidized bed pressure-temperature swing adsorber to recover CO_2 from flue gas. Simulation performed at various riser operating condition to see its effect on purity and recovery.

Main benefits are associated from combination of PSA and TSA for development process efficiency and guaranty the replication of the adsorption-desorption process in various cycles. In PTSA process the operating cost can be reduced because of the lower regeneration temperature than that is in conventional TSA and because of using normal regeneration pressure than that of vacuum conditions required in VSA process [14].

In this work, a commercial unit of PTSA established in South Pars Complex in the Middle East is simulated for desulfurization of natural gas. The objective of this work is to simulate and study the dynamic behavior and performance of a commercial PTSA process for purification of wet natural gas from mercaptans. A non-isothermal dynamic model incorporating mass, energy and pressure changes has been applied to predict the process dynamics. Natural gas with fractions of heavier hydrocarbons, carbon dioxide, water vapor, and mercaptan impurities is the feed of the PTSA cyclic process with six beds, two-layer adsorption process. Activated alumina due to high polarity has been chosen as the first layer especially for H_2O adsorption [15] and 13X Zeolite as one of selective adsorbents for mercaptans has been considered as the second layer [3], [16], in this process.

2. THEORY

2.1. Mathematical modeling

To understand the dynamic behavior of the adsorption columns, the mathematical models were developed on the base of following assumptions:

- The gradient of the concentration and temperature in the radial and angular direction is neglected.

- The dynamic behavior of the fluid obeys axial dispersion plug flow model in the bed.
- The flow velocity is varied along the bed and it is calculated from total mass balance equation.
- The gas property is described by Peng-Robinson equation of state.
- Diffusion and adsorption into the particles is assumed as a lump kinetic transfer model.
- The mass transfer rate is represented by the linear driving force model between the saturated and loaded solid concentrations.
- The pressure drop is considered along the bed as Ergun equation.
- The adsorption columns operate under adiabatic condition that is provided in the real industrial scale.
- The temperature distribution through the adsorbent was neglected and considered as a lump model.
- The heat capacities of the adsorbent and adsorbate phase are assumed constant.
- The heat of adsorption varies with the surface coverage. However, because the variation of heat of adsorption is small in the experimental range, it is assumed to be constant in the study.

Above assumption was widely accepted by numerous adsorption studies [17-19].

2.1.1. Equations of state

Because of the high pressure and temperature and their changes during the process, gas follows non-ideal behavior so the gas properties such as density and viscosity are obtained from Peng-Robinson equation of state [20].

2.1.2. Mass balance

Based on the preceding assumptions, the component and overall mass balances in the bulk phase of the adsorption column are as follow:

$$\varepsilon \frac{\partial C_i}{\partial t} = -\frac{\partial (uC_i)}{\partial z} + \varepsilon D_{ax,i} \frac{\partial^2 C_i}{\partial z^2} - (1-\varepsilon)\rho_s \frac{\partial q_i}{\partial t} \quad (1)$$

$$\varepsilon \frac{\partial C}{\partial t} = -\frac{\partial (uC)}{\partial z} - (1-\varepsilon)\rho_s \sum_{1}^{n_c} \left(\frac{\partial q_i}{\partial t}\right) \quad (2)$$

Where C_i and q_i are, respectively, concentration of components in the gas phase and in the adsorbed phase, z is axial coordinate in the bed, D_{ax} is the effective axial dispersion coefficient, u is the Superficial gas velocity, ρ_s

is the adsorbent density, n_c is the number of the adsorbed components in the mixture and ε is the bed porosity. The value of D_{ax} is calculated through the following equation [21]:

$$\frac{\varepsilon D_{ax,i}}{D_{m,i}} = 20 + 0.5\, Sc_i\, Re \qquad (3)$$

Where $D_{m,i}$ is the molecular diffusivity of component *i* in the mixture, which is calculated in the appendix, *Re* is the Reynolds number and Sc is the Schmidt number. Referring to the assumptions, the solid linear driving force (LDF) model is used to describe the mass transfer rate of the gas and solid phase [22-23]:

$$\frac{\partial q_i}{\partial t} = k_i(q_i^* - q_i) \qquad (4)$$

Where k_i is the overall mass transfer coefficient, q_i^* is the equilibrium concentration of *i*th component in the adsorbed phase. The overall mass transfer coefficient, k_i, is a lumped parameter considering different mass transfer properties. The overall resistance parameter, $\frac{1}{k_i}$, is calculated under the assumption of film and pore fluid mass transfer resistance as follow [24]:

$$\frac{1}{k_i} = \frac{r_p}{3k_{f,i}} + \frac{r_p^2}{15\varepsilon_p\, K_{p,i}} \qquad (5)$$

Where r_p is the adsorbent radius, ε_p is the adsorbent porosity and the pore diffusivity, $K_{p,i}$ is defined as Knudsen and molecular diffusion coefficients as follow:

$$\frac{1}{K_{p,i}} = \tau\left(\frac{1}{D_{K,i}} + \frac{1}{D_{m,i}}\right) \qquad (6)$$

Where τ is the Tortuosity factor and is a function of solid porosity as below [25]:

$$\tau = \varepsilon_p + 1.5\left(1 - \varepsilon_p\right) \qquad (7)$$

$D_{K,i}$ is the Knudsen diffusion coefficient as follow [26]:

$$D_{K,i} = 97 r_{pore}\left(\frac{T}{M_i}\right)^{0.5} \qquad (8)$$

Where r_{pore} is pore radius, *T* is gas temperature and *M* is molecular weight. The film resistance coefficient $k_{f,i}$ is obtained from the Sherwood number as:

$$k_{f,i} = \frac{sh_i D_{m,i}}{2r_p} \qquad (9)$$

Where the Sherwood number sh_i was estimated with the correlation of Wakao and Funazkri [27]:

$$sh_i = 2 + 1.1Sc_i^{1/3}Re^{0.6} \quad (10)$$

The pressure drop equation is defined by the Ergun's equation as [26]:

$$\frac{\partial P}{\partial z} = -\left(\frac{37.5\,(1-\varepsilon)^2\mu u}{\left(r_p\varphi\right)^2\varepsilon^3} + 0.875\rho\,\frac{(1-\varepsilon)u^2}{r_p\varphi\varepsilon^3}\right) \quad (11)$$

Where P is the local pressure at z axial coordinate, μ is the gas viscosity, φ is shape factor and ρ is the gas density.

2.1.3. Energy balance

Variation of temperature is taken into account because of exothermic adsorption as well as cooling and heating effect by the feed/purge gas stream into the bed. Because of the insulated conditions around the column in industrial scale, the bed was assumed as adiabatic system. The energy balances were considered for the solid and gas phases as follow:

Gas phase:

$$\varepsilon K_{ax}\frac{\partial^2 T}{\partial z^2} - u\rho C_{pg}\frac{\partial T}{\partial z} - \varepsilon\rho\, C_{pg}\frac{\partial T}{\partial t} - a_p(1-\varepsilon)h_i(T-T_s) = 0 \quad (12)$$

Where K_{ax} is the effective axial bed thermal conductivity, T_s is the adsorbent temperature, a_p is the specific area of adsorbent, h_i is the heat transfer coefficient between gas and adsorbent and C_{pg} is the gas mixture heat capacity which was calculated by an equation in appendix. K_{ax} was estimated according to following equation [21]:

$$\frac{K_{ax}}{K_g} = 7 + 0.5PrRe \quad (13)$$

Where Pr is the Prandtl number and K_g is the thermal conductivity of gas mixture which was calculated by an equation in appendix.

Solid phase:

$$\rho_s C_{ps}\frac{\partial T_s}{\partial t} = \rho_s\sum_{i=1}^{n_c}(-\Delta H_i)\frac{\partial q_i}{\partial t} + a_p h_i(T-T_s) \quad (14)$$

Where C_{ps} is the heat capacity of adsorbent, and ΔH_i is the heat of adsorption of *i*th component.

The internal heat transfer coefficient h_i is obtained from below equation:

$$h_i = \frac{Nu_i k_i}{2r_p} \quad (15)$$

Where Nu is the Nusselt number and defined by the following equation [27]:

$$Nu_i = 2 + 1.1 Pr_i^{1/3} Re^{0.6} \quad (16)$$

2.2. Adsorption isotherms and heat of adsorption

Gaseous feed consists of many impurities, but in this study, carbon dioxide, water vapor, heavy hydrocarbons (C_{+3}) and mercaptans are considered as the impurities and absorbable species, whereas methane and ethane are considered as non adsorbed part of natural gas on the surface of activated alumina and 13X. Among the impurities, water vapor, mercaptan have higher adsorption tendency toward 13X zeolite because of their polar surface properties [2-3, 28]. Presence of water vapor and to some extent carbon dioxide lowers down the zeolite affinity towards light mercaptans. In addition, at higher pressures heavy hydrocarbons have relatively strong affinity toward 13X and reduce mercaptan adsorption capacity [29]. On the other hand, activated alumina can strongly adsorb water with high capacity and then carbon dioxide with lower capacity, but the other components have ignorable adsorption capacity (in the operating pressure zone the amount of water adsorption on alumina is approximately three time more than carbon dioxide, and carbon dioxide adsorption is about three time more than both mercaptan and propane) [15, 30-31]. In this work, the water vapor and carbon dioxide isotherms on 13X and activated alumina are taken from work of Ferreira et al. [15]. The mercaptans in feed were assumed as a lumped component with the properties of ethyl-mercaptan because most of the mercaptans in natural gas are close to this material. The isotherm data of ethyl-mercaptan were taken from the work of Weber et al. [2]. Heavy hydrocarbons considered as a lump component similar to propane and the data was taken from Da Silva et al. work [29]. In this study, the isotherm of water vapor on activated alumina was better fitted by Dubinin-Astakhov equation [32] rather than Langmuir. Dubinin-Astakhov equation for single component is written as following:

$$\frac{q_i^*}{q_{m,i}} = \exp\left(-\left(\frac{RT}{E_i}\ln\left(p_{0i}/p_i\right)\right)^m\right) \quad (17)$$

Where p_i is the *i*th component partial pressure, p_0 is the *i*th component saturation pressure, $q_{m,i}$ is the *i*th component maximum capacity and is constant, E is the characteristic energy and m represents the surface heterogeneity.

The extended Langmuir equation has been chosen as isotherm model for the equilibrium adsorption of each component from the gas mixture, as follow [32]:

$$\frac{q_i^*}{q_{m,i}} = \frac{B_i p_i}{1 + \sum_{j=1}^{n} B_j p_j} \qquad (18)$$

In this equation, B_i and $q_{m,i}$ are respectively adsorption parameter and maximum capacity of each component. These parameters were predicted by least square regression of Langmuir equation on the single isotherm experimental data to achieve the minimum sum of square of error between adsorbed amount of the model and experiment. This algorithm was performed for each component in each temperature. The fitted parameters were obtained for different temperatures and the temperature relation of the parameters was determined by regression analysis of the parameters with temperature by Arrhenius equation as the following:

$$B_i = B_{0,i} \exp\left(-\frac{\Delta H_i}{RT}\right) \qquad (19)$$

B_{0i} and ΔH_i are called pre-exponential and adsorption energy constant, respectively, and they are predicted from isotherm data derived at different temperatures. Isotherm constants and heat of adsorption of each component are derived by regression of appropriate models on the experimental data and they are tabulated in Table 1.

Table 1.

3. PROCESS DESCRIPTION

In this plant, each train comprises six two-layer adsorption insulated columns which work with co-current pressurization by the inlet natural gas feed. Figure 1 is a simple diagram of the sequential process description. Inlet gas flows downward through the three parallel beds at high pressures for adsorption while the other beds are working at lower pressures and high temperatures for the regeneration mode. Feed flow rate to each bed is about 2.2 kmol/s, at 302 K and 6.8 Mpa. The specification of the inlet feed is shown in Table 2.

Figure 1.

Table 2.

Approximately 6% of the purified product was used for the bed regeneration as the purge feed. In the regeneration step, the bed is firstly depressurized from 6.8 to 1.2 Mpa. The purified gas passes through the hot regenerated bed to cool down the bed. After cooling the specified bed, the outlet stream is heated up to 590 K by a heat exchanger, and passes through another the column undergoing heating stage from 480 K to 590 K. Thereafter the outlet gas passes through a second column to heat up the column from ambient temperature to 480 K, as shown in Figure 1. Each cycle takes 36 hours to be accomplished and there are 18 hours time for adsorption, 17 hours for desorption mode and one hour for the rest.

In each cycle, each bed undergoes the following cycle stages and the bed inter-connection sequence for the six bed PTSA process is presented in Figure 2.

(I) Down flow high-pressure, low-temperature adsorption
(II) Counter current depressurization
(III) First high-temperature low-pressure countercurrent desorption
(IV) Second high-temperature low-pressure countercurrent desorption
(V) Low-temperature low-pressure countercurrent cooling
(VI) Low-temperature, co-current pressurization with feed

Figure 2.

Each bed consists of two layers of activated alumina and 13X zeolite, in which activated alumina is placed at the top layer of each column. Characteristics of the adsorbents and columns are listed in Table 3.

Table 3.

The process operating condition and the time duration of each step are brought in Table 4. The graphical changes of controlled operating pressure and temperature during one cycle, in each step are shown in Figure 3, versus the time.

Table 4.

Figure 3.

4. NUMERICAL SOLUTION

All of the mass and energy balances with appropriate initial and boundary conditions would be solved versus time and length of the bed to achieve the species concentrations and temperature in fluid and solid phase, density, velocity and pressure changes versus time and length of the bed in each step. The initial conditions as well as boundary conditions considering the inlet and outlet conditions are presented as following [24], [26]:

Co-current pressurization:

$$t = 0:\ C_i = C_{iR,n_{cycle}-1}\ , q_i = q_{iR,n_{cycle}-1}\ , T = T_{R,n_{cycle}-1} \qquad (20)$$

Where $n_{cycle}$is the number of cycle. Pressurization step is implemented by the feed stream as a concurrent direction with the adsorption step. In this process, the pressure is controlled by a linear function of time and the pressure is reached to its ultimate value during the pressurization step and is defined by the following equation:

$$P = \frac{P_H - P_L}{time_p} t + P_L \qquad (21)$$

Pressurization and depressurization steps take only 0.5 hours that is very short time compared with the adsorption and regeneration time. Linearity or nonlinear behavior of the pressure had no significant effect on efficiency of the process in this short time, therefore the pressure dependency was assumed linear.

Where $time_P$ is the time of pressurization step.

$$\begin{cases} z = 0:\ \frac{\partial(C_i)}{\partial z} = 0\ ,\ \frac{\partial T}{\partial z} = 0\ , u = 0 & (22) \\ z = L:\ \frac{\partial(C_i)}{\partial z} = \frac{u}{D_{ax,i}}\left(C_{F,i} - C_i\right), \frac{\partial T}{\partial z} = \frac{uc_{pg}P}{K_{ax}RT}(T - T_F) \quad P = P_F & (23) \end{cases}$$

Adsorption stage:

$$t = 0: C_i = C_{iP,n_{cycle}} q_i = q_{iP,n_{cycle}}\ , P = P_F\ , T = T_F \qquad (24)$$

$$\begin{cases} z = 0:\ \frac{\partial(C_i)}{\partial z} = 0\ , \frac{\partial T}{\partial z} = 0 & (25) \\ z = L:\ \frac{\partial(C_i)}{\partial z} = \frac{u}{D_{ax,i}}\left(C_{F,i} - C_i\right)\ ,\ \frac{\partial T}{\partial z} = \frac{uc_{pg}P}{K_{ax}RT}(T - T_F)\ , P = P_F\ , u = u_F & (26) \end{cases}$$

Depressurization stage:

$$t = 0: C_i = C_{iAn_{cycle}}, q_i = q_{iAn_{cycle}}, T = T_{An_{cycle}} \quad (27)$$

In this step, bed pressure is decreased with a linear function of time and it's controlled using the time of depressurization step by the following equation:

$$P = -\frac{P_H - P_L}{time_d} t + P_L \quad (28)$$

Where $time_D$ is the time of depressurization step.

$$\begin{cases} z = 0: \frac{\partial(C_i)}{\partial z} = 0 \ , \frac{\partial T}{\partial z} = 0 \ \ , u = 0 & (29) \\ z = L: \frac{\partial(C_i)}{\partial z} = 0 , \frac{\partial T}{\partial z} = 0 \ , \ \mathrm{P} = \mathrm{P}\big|_{\mathrm{z}=\mathrm{L}} & (30) \end{cases}$$

Countercurrent regeneration stage:

$$t = 0: C_i = C_{iD,n_{cycle}}, q_i = q_{iD,n_{cycle}}, T = T_{D,n_{cycle}} \quad (31)$$

$$\begin{cases} z = 0: \ \frac{\partial(C_i)}{\partial z} = -\frac{u}{D_{ax,i}}(C_i - 0), \frac{\partial T}{\partial z} = \frac{uc_{pg}P}{K_{ax}RT}(T - T_F), u = u_R \ , \mathrm{P} = \mathrm{P_R} & (32) \\ z = L: \frac{\partial(C_i)}{\partial z} = 0 , \frac{\partial T}{\partial z} = 0 & (33) \end{cases}$$

Where the subscripts F, H, L, A, R, D, and P represent the feed, high pressure, low pressure, adsorption, regeneration, depressurization and pressurization, respectively and *L* is the length of bed.

Numerical solution of the nonlinear parabolic PDEs derived from mass and energy balances were conducted by implicit method of lines using finite difference method for the spatial derivatives. Firstly the second and first space derivatives were discreted by central and upwind- differential scheme (backward), respectively. In this way, the sets of partial equations were transformed to the sets of ODEs with respect to the time derivative terms. The length of the bed was divided to 20 increments and the set of equations were solved by Implicit Euler method with the time step of one second. Using upwind- differential scheme for the first order derivative of space and implicit Euler method for ODE solution can guarantee the stability of the numerical solution [33-34].

Cyclic steady-state convergence

The one bed adsorption is a dynamic process, whereas in the cyclic adsorption process the steady state condition can be achieved after passing some cycles, therefore the extract and raffinate compositions become constant and no change is occurred versus the time. Therefore a cyclic steady state (CSS) can be defined, for the same position in each cycle and the dependent variables remain constant with respect to the consecutive cycle. In the present work, the condition to approach to the CSS was defined as the total adsorbed amount in adsorption step between two subsequent cycles as following formula.

$$\left|\int_0^L q_i dz\right|_{n_{cycle}-1} - \int_0^L q_i dz\Big|_{n_{cycle}}\Bigg| < \delta \qquad (34)$$

Where convergence parameter, δ in the above equation has been considered as 10^{-5}. This condition was selected as the stop criteria of simulation, and then the results were reported.

5. RESULTS AND DISCUSSION

The commercial PTSA cyclic process of mercaptan removal unit (MRU), established in South Pars Complex region, was simulated and profiles of the concentrations and temperature of fluid phase and solid phase were determined versus length of the beds and time variation. It was revealed that after about seven sequential running cycles the steady condition was achieved. The results are presented in Figure 4a and 4b to observe the time variation of solid temperature and adsorbed amount, respectively, at the top of the bed. Because this process is about purification from natural gas and most of the gaseous feed doesn't adsorb on the adsorbents, there are few cycles required to reach to the stable conditions especially that regeneration occurs by high temperature and high purge flow rate, therefore the pores of the solid are desorbed from impurities and the bed is returned to its fresh condition. However the unsteady conditions may arise according to the temperature change and energy accumulation in the bed, appropriate cooling flow rate in a high time duration is used for cooling the bed after regeneration, therefore the identical temperature to the initial condition can be occurred in the beds. In this process the time for cooling bed is as long as four hours and it seems to be appropriate condition for cooling the beds.

Figure 4.

In the following sections validation of simulation, the paramaetric analysis of the model towards operational conditions are presented and a new strategy would be suggested for the sake of energy saving.

All the required physical properties and model parameter for simulation were derived from the appropriate equations that are shown in the Appendix.

5.1. Validation

The computed outlet mercaptan and water vapor composition from adsorption stage and two heating stages have been compared with the available real results from the process in Figure 5, and subsequently the relative error of each result is presented in Table 5. The relative errors are around 5 to 10% for different stages, and the simulated results are in a good agreement with the real responses.

Figure 5.

Table 5.

In addition the breakthrough curve of mercaptan resulted from simulation compared with that of real plant is presented in Figure 6. As can be seen the simulated breakthrough curve of mercaptan is in good agreement with real plant data.

Figure 6.

5.2. Simulation results

5.2.1. Breakthrough curves

The breakthrough curves are presented in Figure 7 for mercaptan, water vapor, C_3 as the heavy hydrocarbons and carbon dioxide at different sections of the bed. The points Z=4.7 m and Z=5 m are located in alumina layer and the other points are located in the 13X layer. As expected, each fraction is increasing versus the time until saturation is reached.

As shown in Figure 7a, at the end of adsorption step (t=18 h) mercaptan concentration is close to 5 ppmv at the bed outlet (Z=0.1 m) and the process meets the mercaptane standard level, lower than 10 ppmv. Water vapor breakthrough curve is observed in Figure 7c in which most of water removal takes place in alumina however traces of water are reached to 13X layer. The breakthrough curves of C_3 and carbon dioxide are presented in Figure 7b and 7d, respectively. The curves show saturation of the bed after 2h working in the adsorption mode

because of much higher concentration of these components in the feed stream. In addition, the role up behavior of C_3 is occurred at the same time of CO_2 adsorption in 13X layer, and shows weaker adsorption affinity of C_3 rather than CO_2. It should be noted that dynamic adsorption of heavy hydrocarbons and CO_2 would be studied in the present simulation because they hinder the proper adsorption of mercaptan and affect the saturation time of the bed.

As mentioned before, activated alumina is located at top of 13X layer to remove all water vapor entering through 13X, however as clearly shown in Figure 7c, some of water vapor is diffused through 13X layer therefore a small part of 13X is prevented from mercaptan adsorption.

Figure 7.

The Adsorbed phase concentration of the components are shown at the beginning, middle, and end of the bed versus cycle time in the sequence of cycle steps (adsorption, depressurization, desorption and pressurization), in Figure 8a, 8b, 8c and 8d. By comparison the adsorbed mercaptan (Figure 8a) with heavy hydrocarbons (Figure 8b) and carbon dioxide (Figure 8d) it is revealed that carbon dioxide and heavy hydrocarbons are fully desorbed at 22.5 h, just a half of first heating step time, whereas the bed is not regenerated from mercaptan and it would be totally desorbed at the second heating stage. It means due to the strong adsorption and high heat of adsorption, second heating stage is required for desorption of mercaptan. As shown in Figure 8c, water vapor also needs 2 h of the second heating stage to be fully desorbed. The priority of alumina layer is clearly shown in Figure 8c for adsorption of water vapor rather than CO_2 adsorption that is shown in Figure 8d.

Figure 8.

5.2.2. Mass transfer zones (MTZ)

Mole fraction profile of each component is presented at the steady condition in the adsorption mode, first and second heating stages for each component at various times for both layer of 13X and activated alumina (AC), in Figure 9a, 9b,9c and 9d. By progressing time, MTZ moves from top to the bottom of the bed. For mercaptan all parts of 13X is participated in adsorption and after 18h MTZ approaches to the end of the bed. The MTZs of CO_2 and heavy hydrocarbons reach to the bottom after 2 h processing and concentration profiles turn to a straight line which means there is no further adsorption.

Figure 9.

MTZ of water vapor is shown in Figure 9c at different cycle times and according to the fact that carbon dioxide and heavy hydrocarbons shortly occupy the bed, water vapor would be the main competitor of mercaptan adsorption in 13 X layer. After 14 h working, water MTZ is expanded from top of AC to the bottom of layer 13X, and interfere the efficiency of the column.

Figure 10 a, 10b, 10c and 10d present the MTZs during bed regeneration (steps III and IV) at different times, from 19 up to 30 h, for the first and second heating stages. Heating stages are carried out by a fraction of the hot product from bottom to top of the bed.

Figure 10.

As can be seen, with progressing time the impurities are exhausted from 13X bottom layer to the AC top layer. It can be seen that after 30 h mercaptan is removed from the bed and after 26 h water vapor is exhausted, however this time is 24 h for CO_2 and HC evacuation. The higher heat of adsorption and higher adsorption tendency of mercaptan to 13X than those for CO_2 and HC, cause time delay for mercaptan evacuation from the bed.

As shown in Figure 10a and 10c at initial times of heating stage, mercaptan and water vapor MTZ show lower gas concentrations than those in later times. By progressing time and heat transfer to the solid, desorption takes place and species concentrations are increased in gas phase until all the species are evacuated from the solid, whereas in Figure 10b and 10d, at the initial times of heating stage significant amounts of CO_2 and HC are released to the gas phase at the initial length of the column, because of their weaker adsorption affinity than those for mercaptan and water vapor.

5.2.3. Solid temperature variation

The temperature variation of the bed versus time is shown in Figure 11 at different stages. In the adsorption mode, at the beginning of the process, temperature increases because of large value of carbon dioxide adsorption and heavy hydrocarbons, while at the next times the temperature is close to the inlet feed. At the depressurization step (II) the temperature is firstly reduced because of pressure reduction and consequently endothermic desorption. At the first heating stage (III), the temperature reduction wave is extended through the bed because of endothermic desorption of carbon dioxide and heavy hydrocarbons that are taking place at the initial times. At the 2nd heating stage (IV), the first part of the bed that is exposed to hot product (Z=0.1) is heated more than the other parts where a lower adsorption had occurred in adsorption stage. For the cooling

stage (V) like heating stage, the beginning part of the bed is exposed to the cold feed therefore temperature reduction occurs faster than other parts. In pressurization stage (VI), the temperature increases because of increasing bed pressure by inducing feed and adsorption taking place.

Figure 11.

5.3. *Parametric analysis*

5.3.1. Effect of feed composition

Composition of the inlet feed significantly affects the quality of the product and sometimes the upstream process may induce variation of feed composition. Figure 12a and 12b provide the effect of carbon dioxide and heavy hydrocarbons inlet composition on mercaptan breakthrough curves, respectively. As can be seen, the effect of HC is much more significant than that of CO_2 on mercaptan adsorption so that a 25% decrease in the heavy hydrocarbons inlet concentration adds about 4 hours to the breakthrough time in adsorption step. The high tendencies of 13X towards HC and carbon dioxide cause occupation of the surface and reduction of mercaptan adsorption ability. Therefore as a recommendation, replacing AC with an adsorbent that can adsorb carbon dioxide as well as water vapor, at the top of the 13X can be beneficial.

Figure 12.

As said earlier, water vapor is a component with substantial effect on mercaptan adsorption and competes with mercaptan in adsorption on 13X. Figure 13a and 13b show the effect of inlet mercaptan and water vapor composition on product purity. As expected, by increasing the inlet concentration of water vapor, mercaptan outlet is increased with the same pre-layer AC height. Comparison of Figure 13a with 13b shows the greater sensitivity of mercaptan adsorption associated with input mercaptan compared with that of water vapor. This is because of the presence of an AC pre-layer which prevents water vapor to enter to 13X layer . Water vapor is preadsorbed by this layer whereas all mercaptans as well as any left water vapor should be adsorbed by 13X. Presence of water vapor up to 60 ppmv in the feed has shown no significant effect on the purity of product in which the outlet mercaptan approaches to only 5ppmv. The results of simulation show that all entering water vapor absorbs by AC and doesn't reach to 13X layer to compete with mercaptan adsorption. Simulation reveals that bed can purify a feed made of 230 ppmv mercaptan and maximum 120 ppmv water vapor to the desired standard level by using the same commercial operational conditions.

Figure 13.

5.3.2. Effect of AC length

AC layer is provided on the top of the bed to adsorb water vapor from natural gas before entering to the second layer. Water vapor content is firstly adsorbed by AC layer and it is inhibited to enter to the second layer of 13X. Therefore the length of AC is an important factor in design of the column. Figure 14 has shown the effect of AC length on mercaptan and water vapor outlet mole fraction. As can be observed, with increasing the height of AC the outlet mercaptan and water vapor fractions are reduced. In the absence of AC the outlet meracptan is increased to more than 30 ppmv, and water vapor outlet approaches to 4 ppmv, whereas in the presence of 75 cm AC on the top of 13X , mercaptan can be reduced to less than 10 ppmv. According to the figure, increasing alumina more than 100 cm has no significant impact anymore on the mercaptan outlet results. It means that for height of 100 cm and more, alumina adsorbs all entering water vapor therefore mercaptan adsorption capacity of 13X will be remained constant and unchanged.

Figure 14.

5.3.3. Effect of pressure in adsorption stage

The effect of adsorption stage pressure in the range of 4.5 to 8 Mpa on mercaptan and water vapor outlet composition is shown in Figure 15. Increasing pressure improves the equilibrium uptake of mercaptan and water vapor, thus the fraction of impurities is reduced by increasing bed pressure, however the influence of pressure on mercaptan adsorption is higher than water adsorption. The results reveal that the high rate of mercaptan removal efficiency by increasing pressure up to 6.8, afterward the rate of change is reduced down, whereas the rate of water adsorption is not significantly pressure dependent especially after 5.2 Mpa. Increasing pressure to achieve lower levels of outlet mercaptan requires higher costs such as compressors power and using expensive valves, so it is very important to find out optimum pressure.

According to the figure, for a target value of mercaptan outlet composition lower than 10 ppmv, we can choose an operational pressure around 6 Mpa as a proper choice to significantly reduce operating costs whereas the commercial process is already working around nominal pressure of 6.8 Mpa. In this way, we can prevent wasting approximately 190 (kw) energy which is equivalent to 38000 $ economical profit in operating cost per each year.

Figure 15.

5.3.4. Effect of purge to feed ratio

As noted earlier, in this process nearly 6% of the product is consumed to regenerate the columns. The feed/purge ratio (γ) is an influential parameter on the regeneration of adsorbents from adsorbed materials and therefore on efficiency of the gas purification. The influence of purge/feed on outlet purity is calculated in the range of 0.2 to 12 % by our simulator and shown in Figure 16. As the results show, by increasing purge/ feed the value of outlet fraction of both water vapor and mercaptan decrease. The rate of regeneration is more sensitive towards mercaptan rather than water vapor. The higher purge/feed accelerates the bed evacuation to the full regeneration of the bed and thus enhancement of the adsorbent efficiency for the next cycle. The results reveal that the purification efficiency doesn't change significantly using more than 4% purge/feed ratio therefore for the more economic design of the commercial process we can suggest a purge stream using 4% product to feed stream for the regeneration step.

Figure 16.

This value is two thirds of current operational value considered for the process, therefore it can be used to increases the gained purified natural gas and to reduce the undesired flue gas. By decreasing purge to feed ratio from 0.06 to 0.04, nearly 1394547 (kmol/year) of purified products can be recovered. Approximately, for each 1000000 (kmol/year) of purified natural gas, almost 22000 ($/year) can be saved, which is a significant amount.

5.3.5. Effect of regeneration temperature

The temperature of the first and second stages is another important parameter on the purification of product. The process temperature is already 480 K at the first heating and 590 K at the second heating stage. The effect of heating temperature on outlet mercaptan fraction is provided in Figure 17a and b. Figure 17a is obtained at different temperature levels of first heating stage and Fig 17b is provided at various temperatures of second heating stage. Each figure is achieved by assuming that heating temperature of the other stage is kept constant at its nominal design.

As shown in the figure, the temperature increase either in the first stage or second stage of heating leads to decrease water vapor and mercaptan outlet fraction. This decreasing trend for mercaptan is more intense, rather than water, in both heating stages indicated greater sensitivity of mercaptan desorption to the temperature. Exceeding temperature of heating stage more than 450 K in the first stage and more than 540 K in the second stage has shown weak effect on the mercaptan removal. In fact, the above mentioned temperatures can be proposed as the economic case for saving energy rather than nominal operational conditions. By replacing the

above temperature, the energy required for heating reduce down from 1650 (kw) to 1400 (kw) which is nearly equal to 11000 ($/year) decrease in operational cost.

Figure 17.

As described in the previous sections, water vapor is almost regenerated in the first stage of heating and the second stage of heating is considered mostly for regeneration of mercaptan. This effect is obvious due to the much lower slop and amount of water outlet mole fraction at the second stage, as shown in Figure 17b.

Further as a suggestion, by finding an optimum temperature and using one heating step, which its duration is equal to the combined duration of two steps, it is possible to approach to the standard allowable mercaptan purification after the cyclic process. Figure 18 shows the mercaptan outlet mole fraction for a one heating stage mode at five different temperatures.

As shown in Figure 18, using just one 12 h heating stage at 500 K also regenerates sufficiently the beds so that bed adsorbs mercaptan under allowance amount in the next adsorption stage. This temperature can be chosen as optimum temperature for when bed uses one heating stage instead of two stages at 480 K and 590 K. Working with this temperature not only leads to save 225 (kw) energy, but also makes the process avoid working with extra facilities.

Figure 18.

5.3.6. Breakthrough curve at new conditions

Finally, the studied operational parameters such as purge to feed ratio, regeneration temperature and adsorption pressure were chosen at the mild condition and they were considered, simultaneously to derive the impurity of outlet natural gas. Using the results obtained from the parametric analysis, instead of using two stages of heating at different temperatures, heating stage was conducted for 12 h in one stage and temperature was fixed at T=510 K, the bed pressure was fixed at 6.1 Mpa and purge/feed ratio was reduced to 0.045. The breakthrough curve of the adsorption stage at mentioned operational conditions are shown in Figure 19, for seven cycles running the simulator and the results reveal that the outlet mercaptan content is under 10 ppmv, which is the maximum allowable value for the process of sulfur removal from natural gas.

Figure 19.

6. CONCLUSIONS

Mathematical modeling of the multi-component dynamic adsorption was performed to remove mecaptan from natural gas in presence of water vapor, carbon dioxide and heavier hydrocarbons. The model was used in a cyclic adsorption process to simulate the commercial process of natural gas purification by PTSA method in the two-layer columns working at six stages per cycle. The adsorbents were commercial activated alumina and 13X with specified properties and isotherm temperature dependent character. Good agreement between the simulated outlet data and real case confirmed capability of the model for simulation of natural gas purification from mercaptan and water vapor in presence of other impurities.

The impact of operational conditions was investigated on the process efficiency by this simulator. It was concluded that the height of AC is a significant design parameter, which should be optimized on the base of feed water content and inlet flow rate to prevent water diffusion to 13X layer to achieve the high efficiency of the process. Sometimes that the feed impurities are overloaded, justification of the operational conditions is required to achieve to the same standard level of sulfur impurities, and therefore the current simulator would be implemented to predict the new conditions.

The adsorption stage pressure, the purge to feed ratio and regeneration temperature were found to be the most effective parameters on sulfur removal efficiency. The results revealed that presence of the other impurities such as carbon dioxide and heavy hydrocarbons diversely affect on mercaptan removal efficiency. In this work, the so-called operational conditions were justified to examine the feasibility of this commercial process for saving more energy. The result of simulation showed that it is possible to save more energy by adjusting operating parameters.

This commercial process is equipped with two-layer adsorbent and is only designed for mercaptan removal, whereas CO_2 removal can be carried out together with mercaptan removal if the bed will be equipped with a third layer, such as activated carbon to adsorb CO_2. In this way, sulfur and CO_2 removal can be conducted simultaneously, and the provided simulator can be used for proper design and further optimization of the new plant.

NOMENCLATURE

a	Heat capacity equation parameter (J/mol/K)
a_p	Specific area of adsorbent (1/m)
A	Thermal conductivity equation parameter
b	Heat capacity equation parameter (J/mol/K)

B_i Affinity constant (1/kpa)

$B_{0,i}$ Affinity constant at infinite temperature (1/kpa)

c Heat capacity equation parameter (K)

C_i Concentration of species i in the gas (mol/m^3)

C_{pg} Heat capacity of gas (J/mol/K)

C_{ps} Heat capacity of adsorbent (J/kg/K)

d Heat capacity equation parameter (J/mol/K)

D Thermal conductivity equation parameter

$D_{ax,i}$ Effective axial dispersion coefficient of species i (m^2/s)

$D_{m,i}$ Molecular diffusivity of species i in mixture (m^2/s)

$D_{K,i}$ Knudsen diffusivity of species i (m^2/s)

$D_{i,j}$ Molecular diffusivity of species j in i (m^2/s)

e Heat capacity equation parameter (K)

E Characteristic energy of the adsorbent (J/mol)

F Thermal conductivity equation parameter

h_i Film heat transfer coefficient between gas and solid ($W/m^2/K$)

ΔH_i Heat of adsorption of species i (J/mol)

K_g Gas thermal conductivity (W/m/K)

$k_{f,i}$ Film mass transfer coefficient of species i (m/s)

$K_{p,i}$ Pore diffusivity of species i (m^2/s)

k_i Overall mass transfer coefficient (s^{-1})

K_{ax} Effective axial thermal conductivity (W/m/K)

k_g' Gas thermal conductivity at atmospheric pressure (W/m/K)

L length of the bed (m)

m Dubinin-Astakhov exponent

M Molecular weight (g/mol)

N Viscosity equation parameter

Nu Nusselt number

n_c Number of the adsorbed components in the mixture

n_{cycle} Number of cycle

n Number of all component in gas mixture

P Pressure (kpa)

Pr Prandtl number

p_i Partial pressure (kpa)

p_0 Saturation pressure (kpa)

P_c Critical pressure (pa)

q_i Adsorbed phase concentration of species i (mol/kg)

q_i^* Equilibrium adsorbed phase concentration (mol/kg)

$q_{m,i}$ Maximum adsorbed phase concentration (mol/kg)

R Ideal gas law constant (J/mol/K)

r_p Adsorbent radius (m)

r_{pore} Pore radius (m)

Re Reynolds number

Sc Schmidt number

Sh Sherwood number

t Time (s)

T Gas temperature (K)

T_s Adsorbent temperature (K)

T_r Reduced temperature

T_c Critical temperature (K)

u Superficial gas velocity (m/s)

V_c Critical molar volume (m^3/kmol)

y_0 Initial mole fraction

y_i Mole fraction of species i

z Axial coordinate in the bed (m)

Z_c Critical compressibility factor

Greek letters

ε Bed porosity

ε_p Adsorbent porosity

τ Tortuosity factor

ρ_s Adsorbent density ($^{kg}/_{m^3}$)

ρ Gas density ($^{mol}/_{m^3}$)

ρ_r Reduced density

μ Gas viscosity (kg/m.s)

μ_0 Gas viscosity at low pressure (kg/m.s)

φ Shape factor

δ Convergence parameter

γ Purge to feed ratio

Subscripts

F Feed
H High pressure
L Low pressure
A Adsorption
R Regeneration
D Depressurization
P Pressurization

REFERENCES

[1] G. Weber, J. P. Bellat, F. Benoit, and C. Paulin, "Adsorption equilibrium of light mercaptans on faujasites," *Adsorption*, vol. 11, pp. 183–188, 2005.

[2] G. Weber, F. Benoit, J. P. Bellat, C. Paulin, P. Mougin, and M. Thomas, "Selective adsorption of ethyl mercaptan on NaX zeolite," *Microporous and Mesoporous Materials*, vol. 109, pp. 184–192, 2008.

[3] J. P. Bellat, F. Benoit, G. Weber, C. Paulin, P. Mougin, and M. Thomas, "Adsorption equilibria of binary ethylmercaptan/hydrocarbon mixtures on a NaX zeolite," *Adsorption*, vol. 14, pp. 501–507, 2008.

[4] M. Kim, J. Jee, Y. Bae, and C. Lee, "Parametric study of pressure swing adsorption process to purify oxygen using carbon molecular sieve," *Industrial & Engineering Chemistry Research*, vol. 44, pp. 7208–7217, 2005.

[5] S. P. Knaebel, D. Ko, and L. T. Biegler, "Simulation and optimization of a pressure swing adsorption system: recovering hydrogen from methane," *Adsorption*, vol. 11, pp. 615–620, 2005.

[6] A. C. Silva and A. E. Rodrigues, "Separation of n/iso-paraffins mixtures by pressure swing adsorption," *Separation and Purification Technology*, vol. 13, pp. 195–208, 1998.

[7] A. Mendes, C. Costa, and A. Rodrigues, "Oxygen separation from air by PSA: Modelling and experimental results: Part I: Isothermal operation," *Separation and Purification Technology*, vol. 24, pp. 173–188, 2001.

[8] S. Bashkova, A. Bagreev, and T. J. Bandosz, "Adsorption of methyl mercaptan on activated carbons," *Environmental Science & Technology*, vol. 36, pp. 2777–2782, 2002.

[9] B. Shirani, T. Kaghazchi, and M. Beheshti, "Water and mercaptan adsorption on 13X zeolite in natural gas purification process," *Korean Journal of Chemical Engineering*, vol. 27, pp. 253–260, 2010.

[10] L. Zhou, M. Yu, L. Zhong, and Y. Zhou, "Feasibility study on pressure swing sorption for removing H2S from natural gas," *Chemical Engineering Science*, vol. 59, pp. 2401–2406, 2004.

[11] W. Cho, K. Lee, and H. Chang, "Evaluation of pressure-temperature swing adsorption for sulfur hexaflouride (SF6) recovery from SF6 and N2 gas mixture, " *Korean Journal of Chemical Engineering*, vol. 28, pp. 2196–2201, 2011.

[12] V. Mulgundmath and F. H. Tazel, " Optimization of carbon dioxide recovery from flue gas in a TPSA system, " *Adsorption*, vol.16, pp. 587-598, 2010.

[13] T. S. Pugsley, F. Berruti, A.Chakma, "Computer simulation of a novel circulating fluidized bed pressure-temperature swing adsorber for recovering carbon dioxide from flue gases, " *Chemical Engineering Science*, vol. 49, pp. 4465–4481, 1994.

[14] J. D. Seader, E. J. Henley, and D. K. Roper, *Separation process principles*, 3rd Ed. New York: Wiley, 2010.

[15] D. Ferreira and R. Magalhães, "Effective adsorption equilibrium isotherms and breakthroughs of water vapor and carbon dioxide on different adsorbents," *Industrial & Engineering Chemistry Research*, vol. 50, pp. 10201–10210, 2011.

[16] A. Ryzhikov, V. Hulea, D. Tichit, C. Leroi, D. Anglerot, B. Coq, and P. Trens, "Methyl mercaptan and carbonyl sulfide traces removal through adsorption and catalysis on zeolites and layered double hydroxides," *Applied Catalysis A: General*, vol. 397, pp. 218–224, 2011.

[17] M. H. Chahbani and D. Tondeur, "Mass transfer kinetics in pressure swing adsorption," *Separation and Purification Technology*, vol. 20, pp. 185–196, 2000.

[18] M. Mehdipour and S. Fatemi, "Modeling of a PSA-TSA process for separation of CH4 from C2 products of OCM reaction," *Separation Science and Technology*, vol. 47, pp. 1199–1212, 2012.

[19] F. A. Da Silva, J. A. Silva, and A. E. Rodrigues, "A general package for the simulation of cyclic adsorption processes," *Adsorption*, vol. 5, pp. 229–244, 1999.

[20] D. Green and R. Perry, *Perry's chemical engineers' handbook*, 8th Ed. New York: McGraw-Hill, 2007.

[21] R. B. Bird, W. E. Stewart, and E. N. Lightfoot, *Transport phenomena*, 2nd Ed. New York: Wiley, 2002.

[22] S. Farooq and D. M. Ruthven, "A comparison of linear driving force and pore diffusion models for a pressure swing adsorption bulk separation process," *Chemical Engineering Science*, vol. 45, pp. 107–115, 1990.

[23] P. Cruz, F. D. Magalhães, and A. Mendes, "Generalized linear driving force approximation for adsorption of multicomponent mixtures," *Chemical Engineering Science*, vol. 61, pp. 3519–3531, 2006.

[24] D. M. Ruthven, S. Farooq, and K. S. Knaebel, *Pressure swing adsorption*, 1st Ed. New York: Wiley-VCH, 1994.

[25] M. Suzuki and J. Smith, "Axial dispersion in beds of small particles," *The Chemical Engineering Journal*, vol. 3, pp. 256-264, 1972.

[26] R. T. Yang, *Gas separation by adsorption processes*. Boston: World Scientific Publishing Company, 1987.

[27] N. Wakao, T. Funazkri, and S. Kaguei, "Effect of fluid dispersion coefficients on particle-to-fluid mass transfer coefficients in packed beds; Correlation of sherwood numbers," *Chemical Engineering Science*, vol. 34, pp. 325–336, 1978.

[28] Y. Wang and M. D. Levan, "Adsorption equilibrium of carbon dioxide and water Vapor on zeolites 5A and 13X and silica gel: pure components," *Journal of Chemical & Engineering Data*, vol. 54, pp. 2839–2844, 2009.

[29] F. A. Da Silva and A. E. Rodrigues, "Adsorption equilibria and kinetics for propylene and propane over 13X and 4A zeolite pellets," *Industrial & Engineering Chemistry Research*, vol. 38, pp. 2051–2057, 1999.

[30] E. Baumgarten, F. Weinstrauch, and H. Hoffkes, "Adsorption isotherms of hydrocarbons on γ-Alumina," *Journal of chromatography*, vol. 138, pp. 347–354, 1977.

[31] R. W. Glass and R. A. Ross, "Surface studies of the adsorption of sulfur-containing gases at 423 .deg.K on porous adsorbent. II. adsorption of hydrogen sulfide, methanethiol, ethanethiol, and dimethyl sulfide on γ-Alumina," *The Journal of Physical Chemistry,* vol. 77, pp. 2571–2576, 1973.

[32] D. D. Do, *Adsorption analysis: equilibria and kinetics*. London: Imperial College Press, 1998.

[33] K. Iusalaas, *Numerical methods in engineering with MATLAB*. Cambridge: Cambridge University Press, 2005.

[34] G. G.Vining, *Statistical methods for engineers*. Pacific Grove: Duxbury Press, 1997.

APPENDIX

A.1.molecular diffusivity

Molecular diffusivity of component *i* in the mixture, $D_{m,i}$, is calculated by the following equation [20]:

$$D_{m,i} = \frac{1 - y_i}{\sum_{x=j}^{n} \frac{y_i}{D_{i,x}}} \qquad (A.1)$$

Where, y_i is the mole fraction of *i*th component and n is the number of total components in gas mixture. The molecular diffusivity of each component through the mixture was assumed as following equation because methane is the dominate component:

$$D_{m,i} = D_{CH_4,i} = D_{i,j} \qquad (A.2)$$

Where $D_{i,j}$ molecular diffusivity of binary gas mixtures was calculated by the Wilke-Lee equation [20].

The amount of molecular diffusivity of each component through the mixture at the adsorption, 1st and 2nd heating stages are brought in Table A1.

Table A1.

A.2.Physical properties prediction and correlation:

Methane is the dominate component of the gas phase, therefore all physical properties are considered as methane property.

Pure gas specific heat capacity C_{pg} has been calculated as follow [20]:

$$C_{pg} = a + b\left(\frac{c}{T} \times \frac{2}{\left(\exp\left(\frac{c}{T}\right) - \exp\left(-\frac{c}{T}\right)\right)}\right) + d\left(\frac{e}{T} \times \frac{2}{\left(\exp\left(\frac{e}{T}\right) + \exp\left(-\frac{e}{T}\right)\right)}\right) \qquad (A.3)$$

Where the coefficients of the above correlation are listed in Table A2.

Table A2.

For prediction of the pure gas viscosity at high pressures following equation was used [20]:

$$\mu - \mu_0 = 5 \times 10^{-11} \frac{M^{\frac{1}{2}} P_c^{\frac{2}{3}}}{T_c^{\frac{1}{6}}} \left(\exp(1.439\rho_r) - \exp(-1.11\rho_r^{1.858})\right) \qquad (A.4)$$

Where P_c, T_c and ρ_r is the critical pressure, critical temperature and reduced density, respectively, μ_0 is the low pressure viscosity according to following equation:

$$\mu_0 = 4.6 \times 10^{-7} \frac{N M^{\frac{1}{2}} P_c^{\frac{2}{3}}}{T_c^{\frac{1}{6}}} \qquad (A.5)$$

Where:

$$N = 0.00034 T_r^{0.94} \quad for\ T_r \leq 1.5 \qquad (A.6)$$

$$N = 0.0001778(4.85T_r - 1.67)^{0.625} \quad for\ T_r > 1.5 \qquad (A.7)$$

Thermal conductivity for pure gas, k_g ,above atmospheric pressure, was calculated by Stiel and Thodos method as follow [20]:

$$k_g = k'_g + \frac{A \times 10^{-4}(e^{F\rho_r} + D)}{\left(\frac{T_c^{\frac{1}{6}} M^{\frac{1}{2}}}{P_c^{\frac{2}{3}}}\right) Z_c^5} \qquad (A.8)$$

ρ_r <0.5 A =2.702 F =0.535 D =-1.000

0.5 <ρ_r>2.0 A =2.528 F =0.670 D =-1.069

2.0 <ρ_r>2.8 A =0.574 F =1.155 D =2.016

Where Z_c is the critical compressibility factor and k'_g *is* gas thermal conductivity at T and atmospheric pressure as follow:

$$k_g = 4.45 \times 10^{-7} T_r \frac{C_{pg}}{\lambda} \qquad (A.9)$$

Where:

$$\lambda = T_c^{1/6} M^{1/2} \left(\frac{101.325}{P_c}\right)^{2/3} \qquad (A.10)$$

A.3. Mass transfer and heat transfer parameters for kinetic adsorption

The average model parameters were calculated by the mentioned equations and they were used in simulation, the adsorption, 1st and 2nd heating stages are listed in Table A3.

Table A3.

Figure Captions:

Figure 1. Schematic diagram of PTSA cycle with six beds and the sequential steps. The three primary beds are at high pressure low temperature mode, the next two beds are in low pressure and high temperature conditions and the last is in low pressure and low temperature.

Figure 2. Bed interconnection sequence for the six-bed multilayer PTSA system.

Figure 3. Operating bed pressure (a); and temperature (b); with elapsed time in a PTSA cycle.

Figure 4. Seven cycles running the simulator to achieve to steady state condition for temperature (a); mercaptan adsorbed amount (b); at top of the bed.

Figure 5. Comparison between simulated results and operational data for the outlet composition of mercaptan and water vapor in natural gas.

Figure 6. Comparison between result of simulation and real plant data for mercaptan breakthrough curve.

Figure 7. Breakthrough curves of mercaptan (a); heavy hydrocarbons (C_3) (b); water vapor (c); carbon dioxide (d); in adsorption stage at various parts of the bed at steady condition.

Figure 8. Adsorbed phase concentration versus time for mercaptan (a); heavy hydrocarbons (b); water vapor (c); carbon dioxide (d); at various part of the bed at steady condition.

Figure 9. MTZ of mercaptan (a); heavy hydrocarbons (b); water vapor (c); carbon dioxide (d); at various times of adsorption stage at steady state condition.

Figure 10. Axial mole fraction in gas phase, mercaptan (a); heavy hydrocarbons (b); water vapor (c); carbon dioxide (d); at various times of the first and second heating stages at steady state condition.

Figure 11. Temperature variation per cycle in various parts of the bed from bottom to top, at steady state condition.

Figure 12. Comparison between breakthrough curves of outlet mercaptan in adsorption mode, for various inlet mole fraction (y_0) of carbon dioxide (a); heavy hydrocarbons (b); at steatdy state condition.

Table captions:

Table 1. Constant isotherm parameters for related adsorbents

	$q_{m,i}(\frac{kmol}{kg})$	$B_{0,i}(1/Mpa)$	$-\Delta H_i(kj/mol)$	$E_i(kj/mol)$	m
Activated alumina					
Water vapor	0.0151	3.22×10^{-7}	60.014	3.72	0.9
Carbon dioxide	0.0011	1.94×10^{-4}	29.805	-	-
Zeolite 13X					
Mercaptan	0.003580	4.32×10^{-8}	65.1624	-	-
Water vapor	0.016842	4.82×10^{-7}	62.5258	-	-
Carbon dioxide	0.005115	3.61×10^{-4}	34.0031	-	-
Propane	0.002821	3.36×10^{-4}	32.5412	-	-

Table 2. Inlet natural gas specification

Parameter	Value
Density (kg/m^3)	0.71
Molecular weight (g/mole)	18.91
Viscosity (Pa.s)	1.37×10^{-6}
Thermal conductivity (W/m.K)	0.035
Water vapor mole fraction(ppmv)	18.2
Mercaptan mole fraction (ppmv)	133.8
CO_2mole fraction (ppmv)	1.0×10^4
Methane mole fraction (ppmv)	95.9848×10^4
Heavy hydrocarbons mole fraction (ppmv)	3.0×10^4

Table 3. Characteristics of the adsorbents and the adsorption columns

	Zeolite 13X	Activate alumina (AC)
properties of adsorbents		
Particle radius (mm)	2.1	2.3
Average macropore radius (nm)	2.44	4.6
BET surface area (m^2/g)	445.6	441.3
Particle void fraction	0.24	0.28
Particle density (g/cm^3)	1.10	1.24
Heat capacity (kJ/kg.K)	1.07	3.85
Tortuosity	1.38	1.36
Shape factor (spherical particles)	1	1
Characteristics of adsorption bed		
Bed length (m)	4.65	0.75
Bed diameter (m)	3.7	3.7
Bed void fraction	0.37	0.26
Bulk density (g/cm^3)	0.69	0.82

Table 4. PTSA process operating conditions

Steps	Flow rate (kmol/s)	Pressure(Mpa)	Temperature (K)	Time(h)
Adsorption step	2.2	6.8	302	18
Depressurization step	-	From 6.8 to 1.2	-	0.5
First heating step	0.134	1.24	480	6
Second heating step	0.134	1.22	590	6
Cooling step	0.134	1.21	302	4
Pressurization step	-	From 1.2 to 6.8	-	0.5
Rest	-	-	-	1

Table 5. Absolute relative error between simulated results and commercial results

Stage	Mercaptan outlet from adsorption stage	Water outlet from adsorption stage	Mercaptan outlet from 1st heating stage	Water outlet from 1st heating stage	Mercaptan outlet from 2nd heating stage	Water outlet from 2nd heating stage
Abs. relative error %	4.9	5.8	7.8	5.3	10.6	9.5

Table A1. Average molecular diffusivity of gases in mixture $D_{m,i}(cm^2/s)$

Stage	Adsorption	1st heating	2nd heating
Mercaptan	1.112×10^{-3}	1.2114×10^{-2}	1.6339×10^{-2}
Water vapor	4.7939×10^{-3}	5.2223×10^{-2}	7.0438×10^{-2}
Carbon dioxide	2.1941×10^{-3}	2.3901×10^{-2}	3.2238×10^{-2}
Heavy hydrocarbons	1.1988×10^{-3}	1.3254×10^{-2}	1.7118×10^{-2}

Table A2. Heat capacity correlation coefficients of methane

	$a\times 10^{-4}(j.mol^{-1}.K^{-1})$	$b\times 10^{-5}(j.mol^{-1}.K^{-1})$	$c\times 10^{-3}(K)$	$d\times 10^{-4}(j.mol^{-1}.K^{-1})$	$e\times 10^{-4}(K)$
CH_4	3.33	0.7993	2.0869	4.16	9.92

Table A3. Model parameters for adsorption kinetic

Step	Zeolite 13X		Activated alumina
adsorption	$\boldsymbol{k_{avg}}$**(1/s)**		
	Water vapor	0.00098	0.00014
	Mercaptan	0.00093	-
	Carbon dioxide	0.00141	0.008205
	Heavy hydrocarbons	0.00731	-
	$\boldsymbol{D_{ax,avg}}(\frac{\boldsymbol{cm^2}}{\boldsymbol{s}})$		
	Water vapor	1.7028	2.4177
	Mercaptan	1.7031	2.4182

	Carbon dioxide	1.7021	2.4171
	Heavy hydrocarbons	1.7025	2.4172
	$\boldsymbol{K_{ax,avg}}(\frac{w}{m.K})$	5.848	5.941
	$\boldsymbol{h_{i,avg}}(\frac{kw}{m^2.K})$	3.1621	4.1246
1st heating stage	$\boldsymbol{k_{avg}}$**(1/s)**		
	Water vapor	0.00991	0.0114
	Mercaptan	0.01565	-
	Carbon dioxide	0.00281	2.2214
	Heavy hydrocarbons	0.0066	-
	$\boldsymbol{D_{ax,avg}}(\frac{cm^2}{s})$		
	Water vapor	1.6742	2.3636
	Mercaptan	1.6764	2.3689
	Carbon dioxide	1.6754	2.3655
	Heavy hydrocarbons	1.6753	2.3651
	$\boldsymbol{K_{ax,avg}}(\frac{w}{m.K})$	0.574	0.598
	$\boldsymbol{h_{i,avg}}(\frac{kw}{m^2.K})$	0.7142	0.903
2nd heating stage	$\boldsymbol{k_{avg}}$**(1/s)**		
	Water vapor	0.0311	0.051
	Mercaptan	0.0592	-
	Carbon dioxide	0.0057	1.1369
	Heavy hydrocarbons	0.0126	-
	$\boldsymbol{D_{ax,avg}}(\frac{m^2}{s})$		
	Water vapor	2.0912	2.9657
	Mercaptan	2.0927	2.9737
	Carbon dioxide	2.0919	2.9682
	Heavy hydrocarbons	2.0899	2.9591
	$\boldsymbol{K_{ax,avg}}(\frac{w}{m.K})$	0.4548	0.4564
	$\boldsymbol{h_{i,avg}}(\frac{kw}{m^2.K})$	0.7541	0.9654

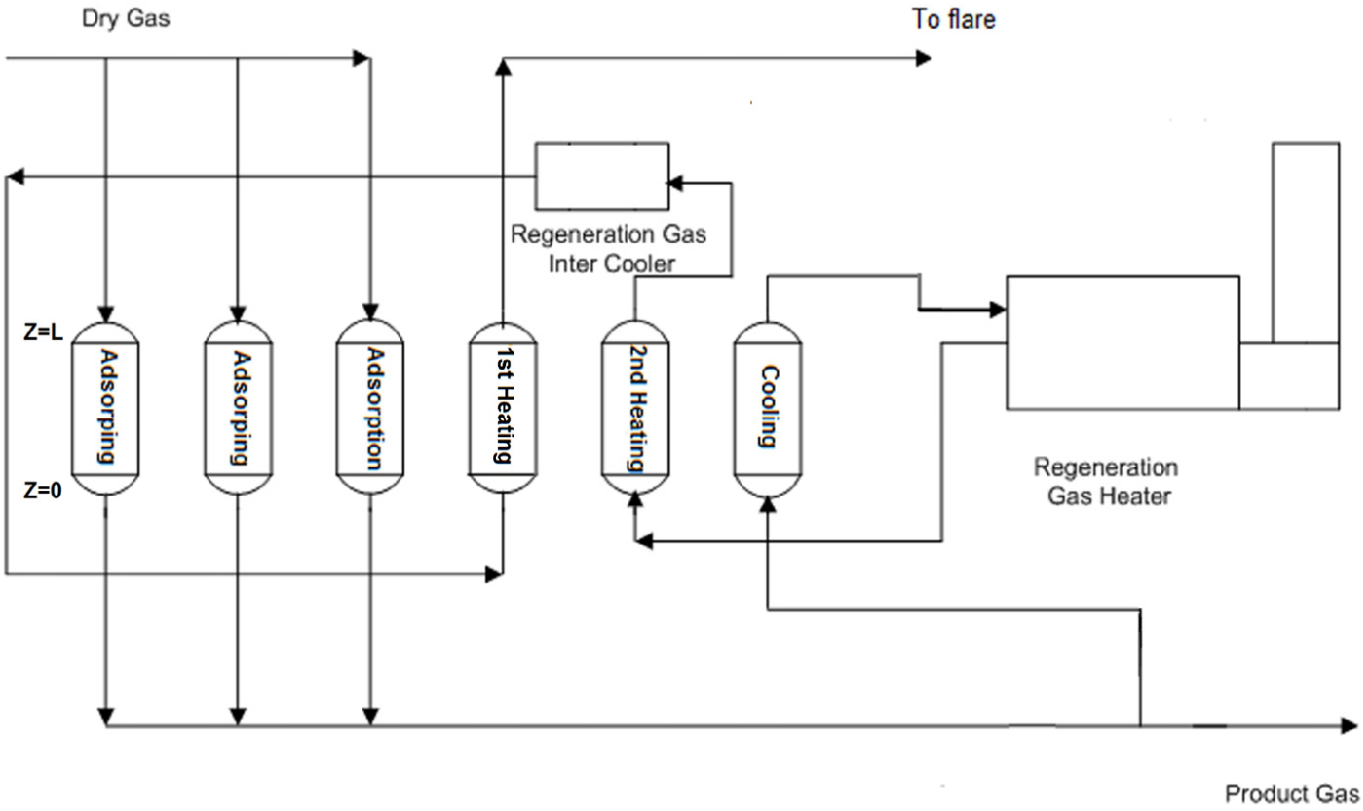

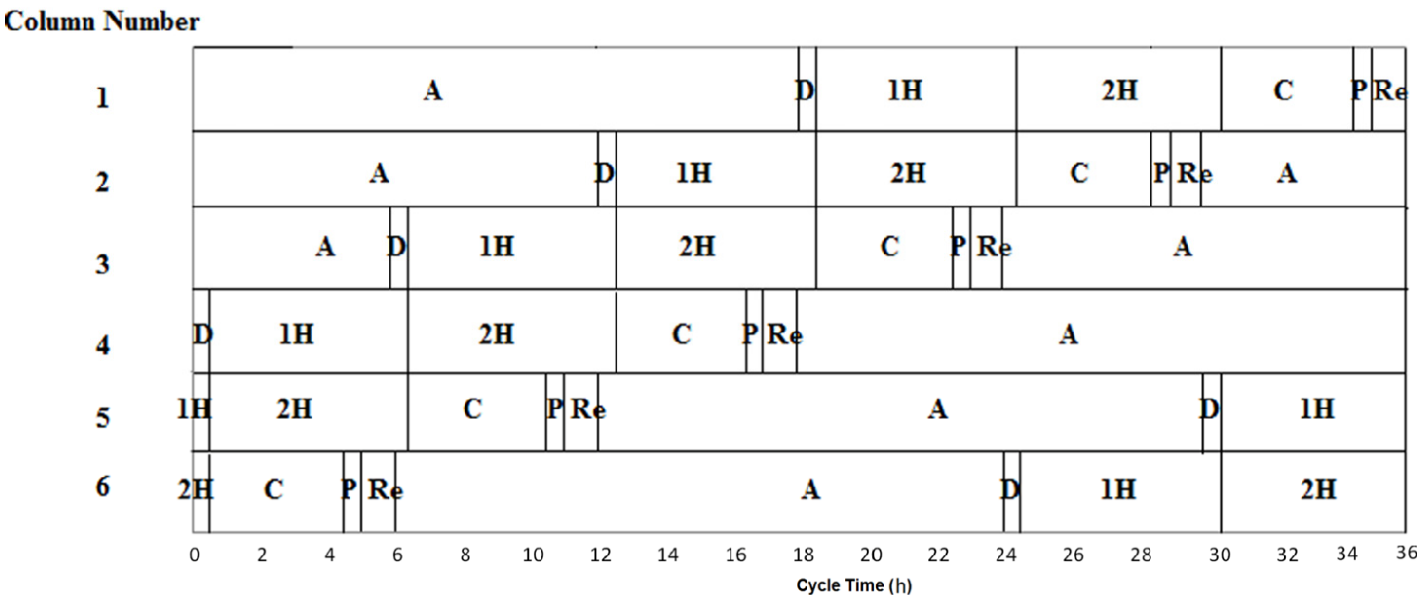

A : Adsorption
D: Depressurization
1H: 1st Heating
2H: 2nd Heating
C: Cooling
P: Pressurization
Re: Rest

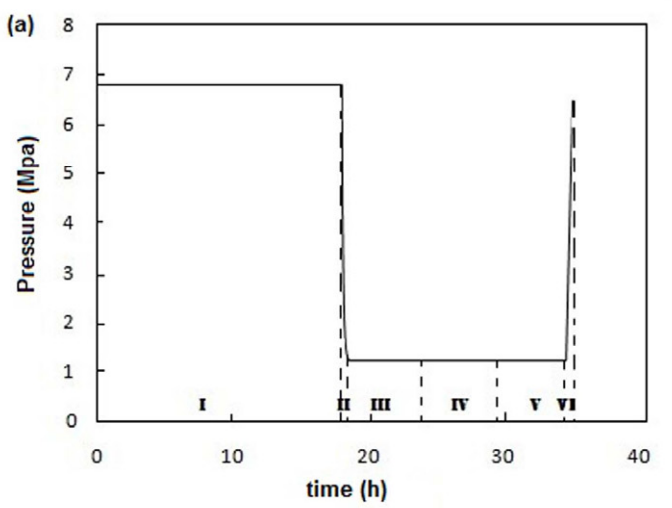

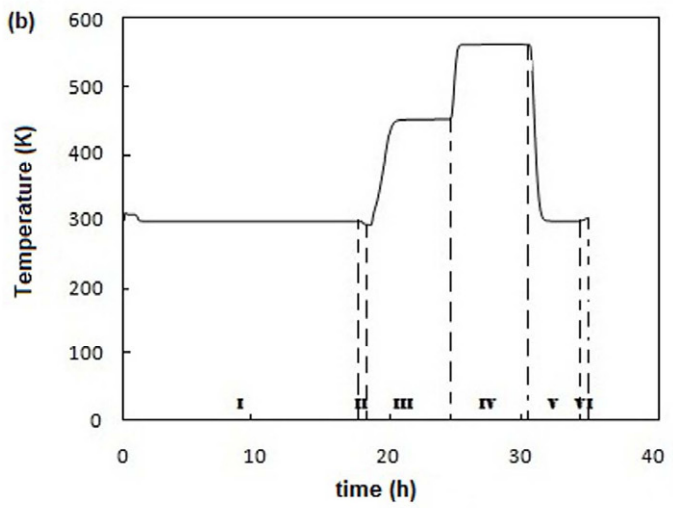

(a)

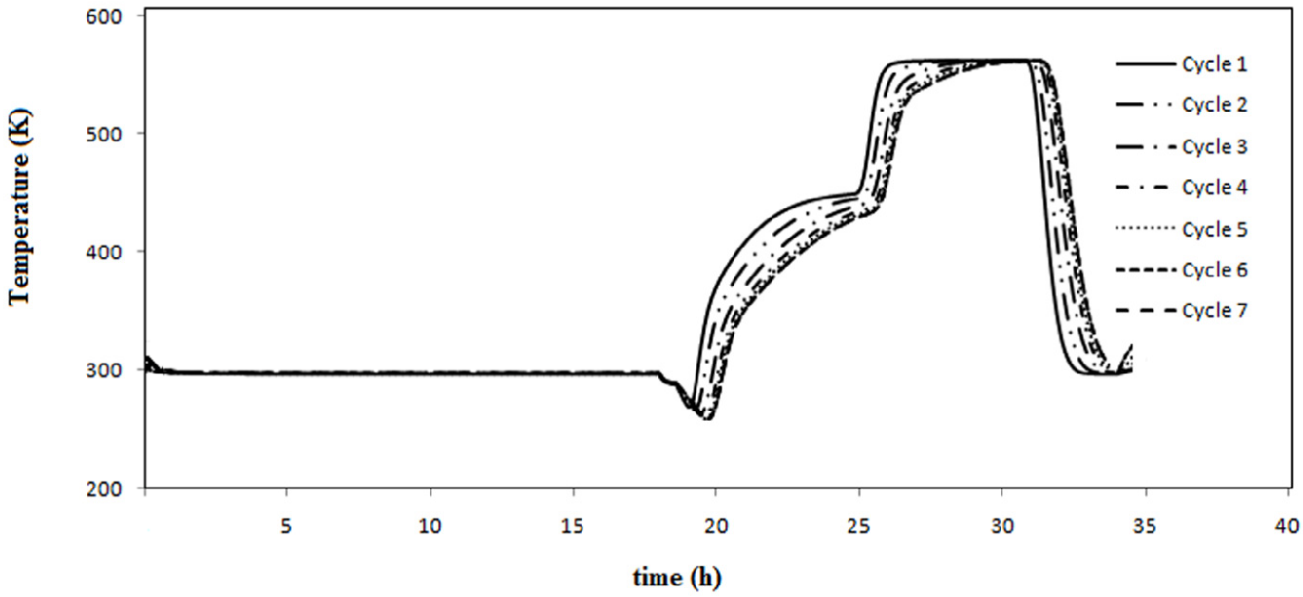
Temperature (K)
600
500
400
300
200
5
10
15
20
25
30
35
40
time (h)
Cycle 1
Cycle 2
Cycle 3
Cycle 4
Cycle 5
Cycle 6
Cycle 7

(b)

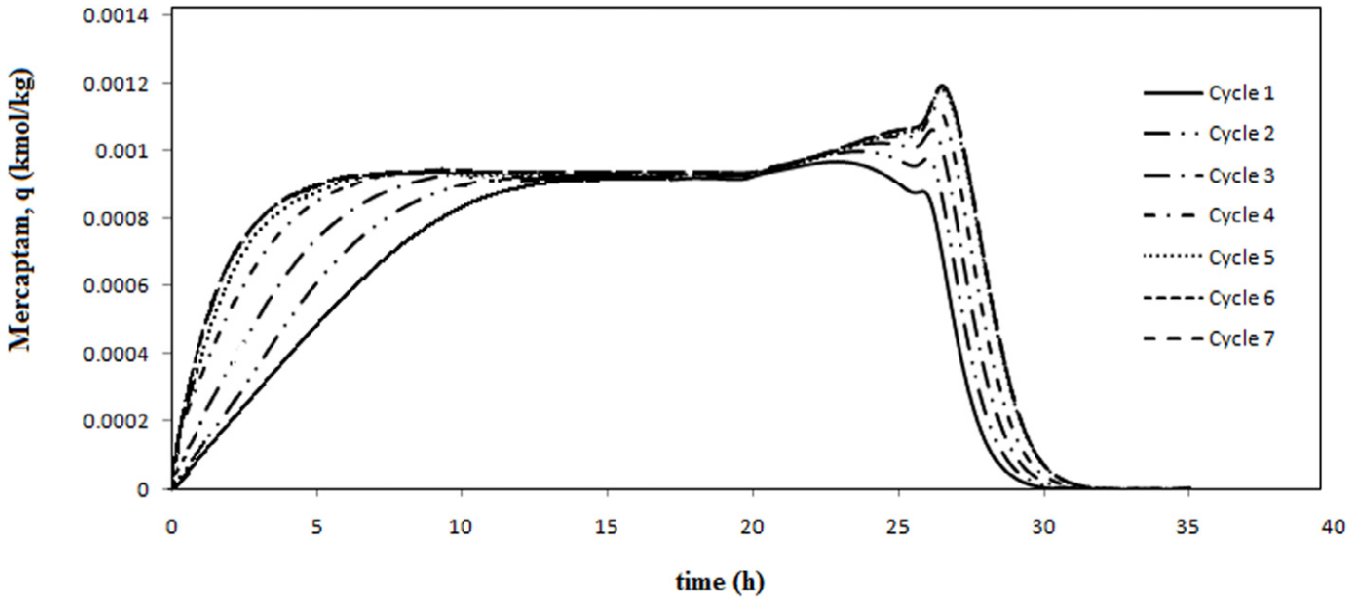
Mercaptam, q (kmol/kg)
0.0014
0.0012
0.001
0.0008
0.0006
0.0004
0.0002
0
0
5
10
15
20
25
30
35
40
time (h)
Cycle 1
Cycle 2
Cycle 3
Cycle 4
Cycle 5
Cycle 6
Cycle 7

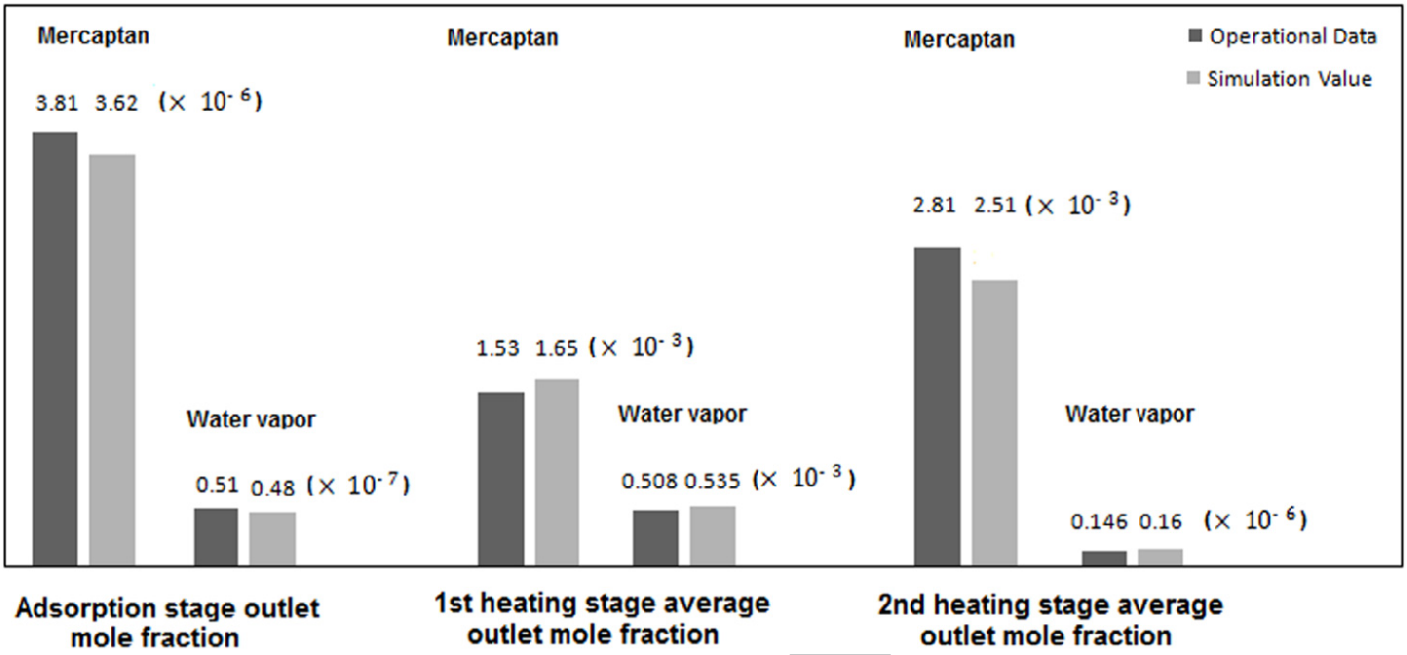

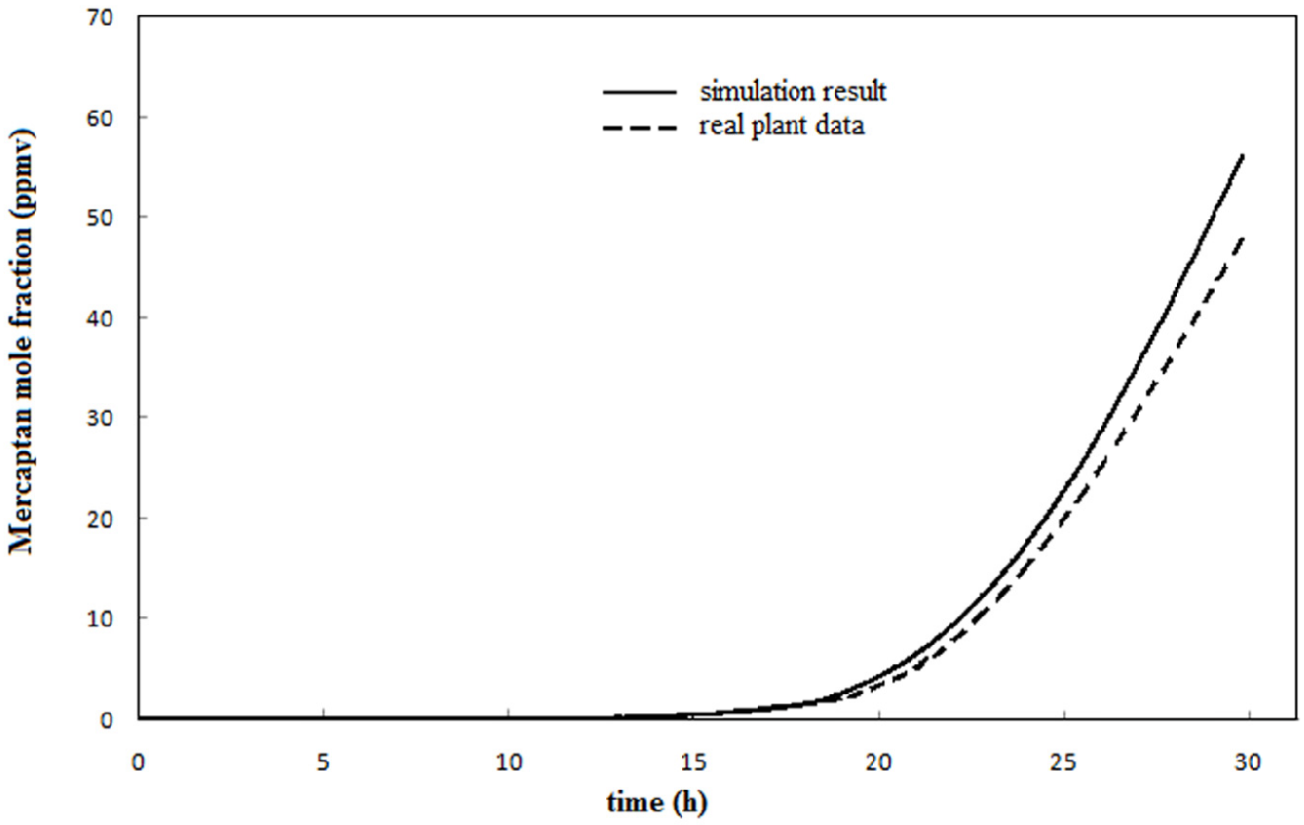

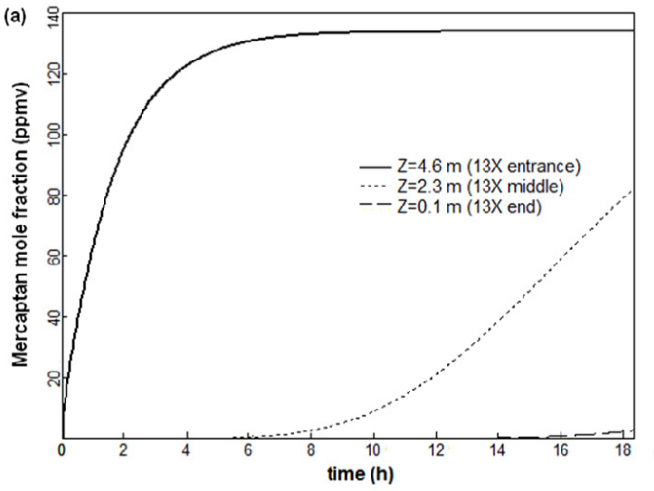

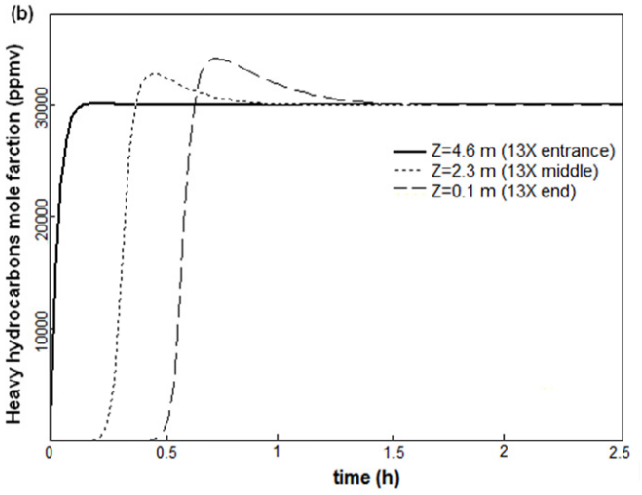

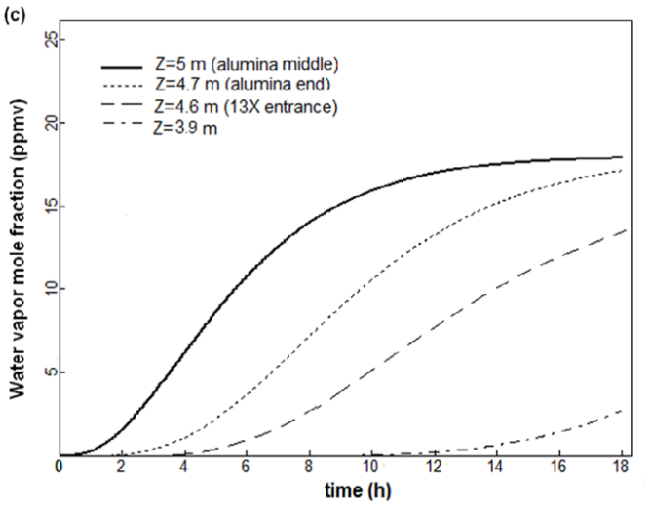

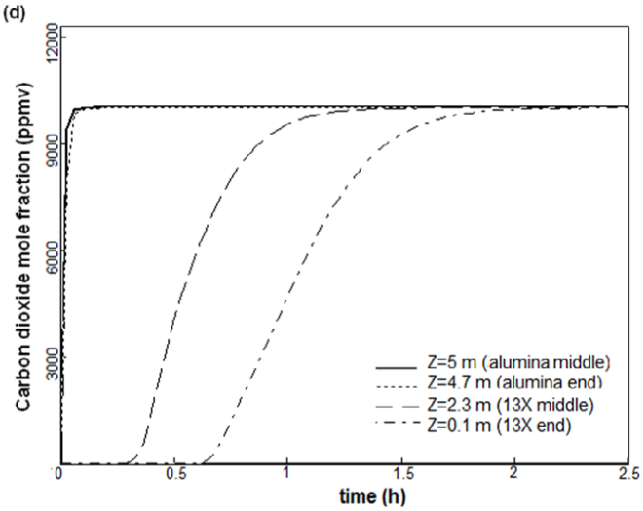

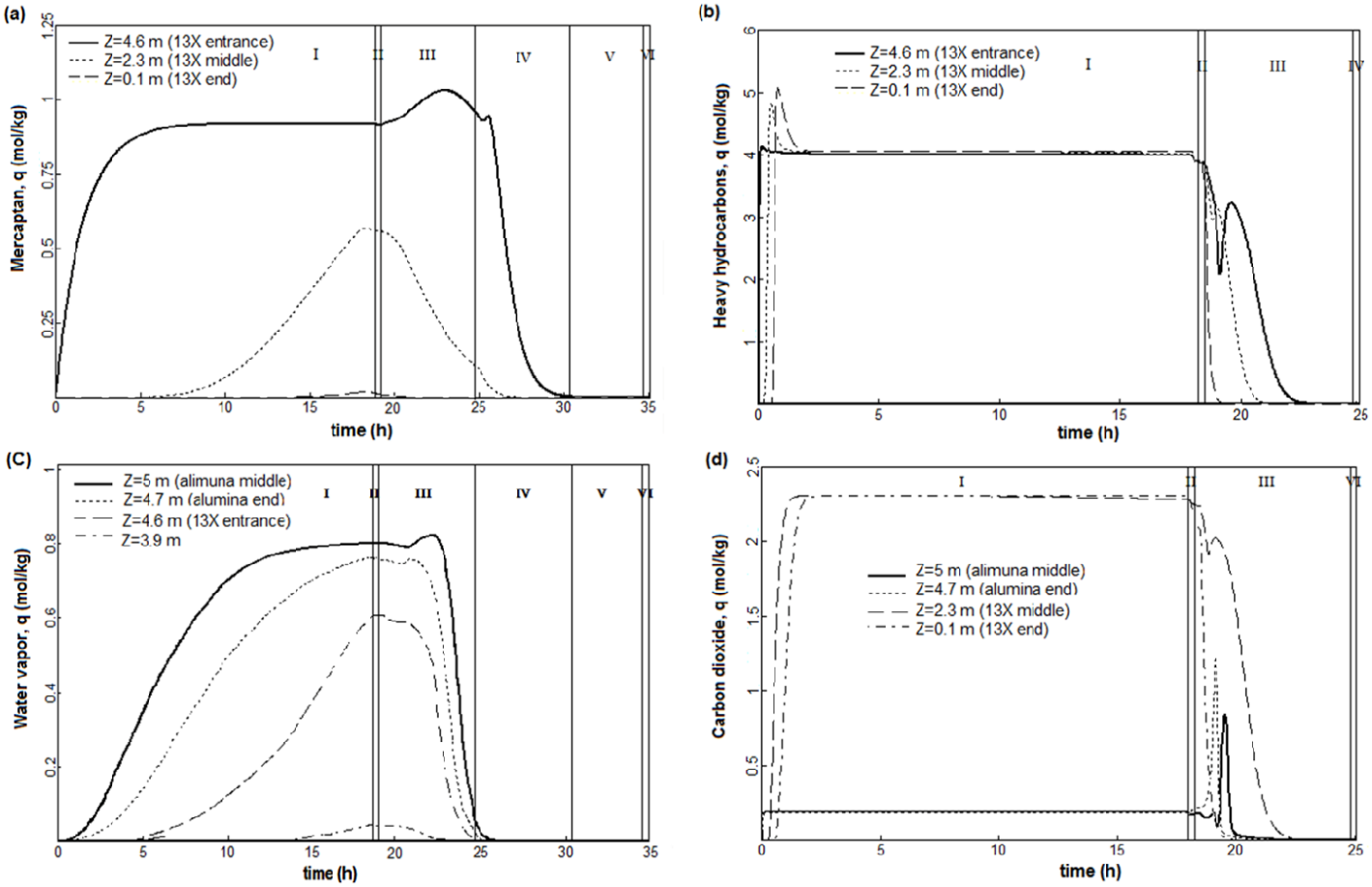

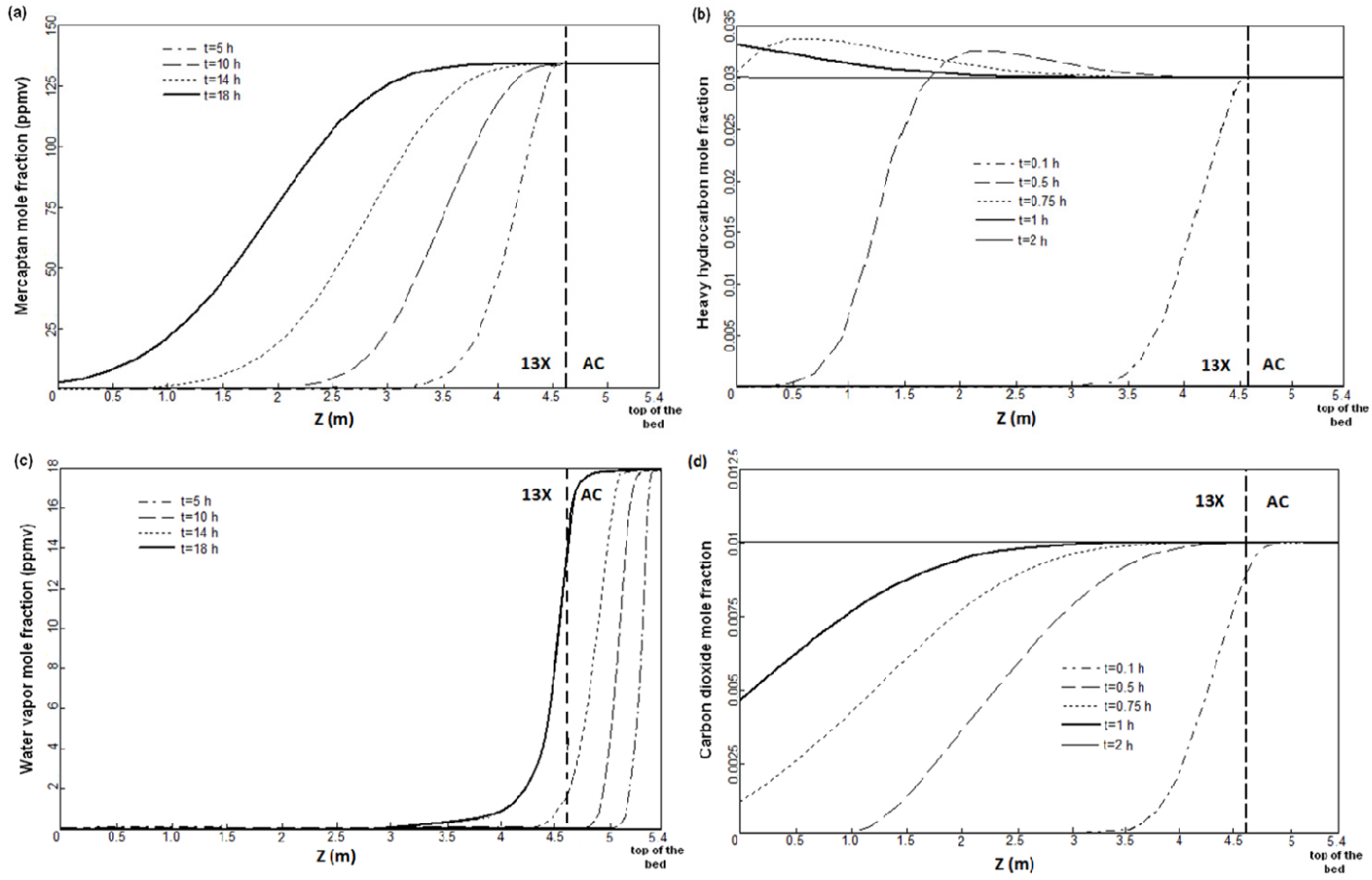

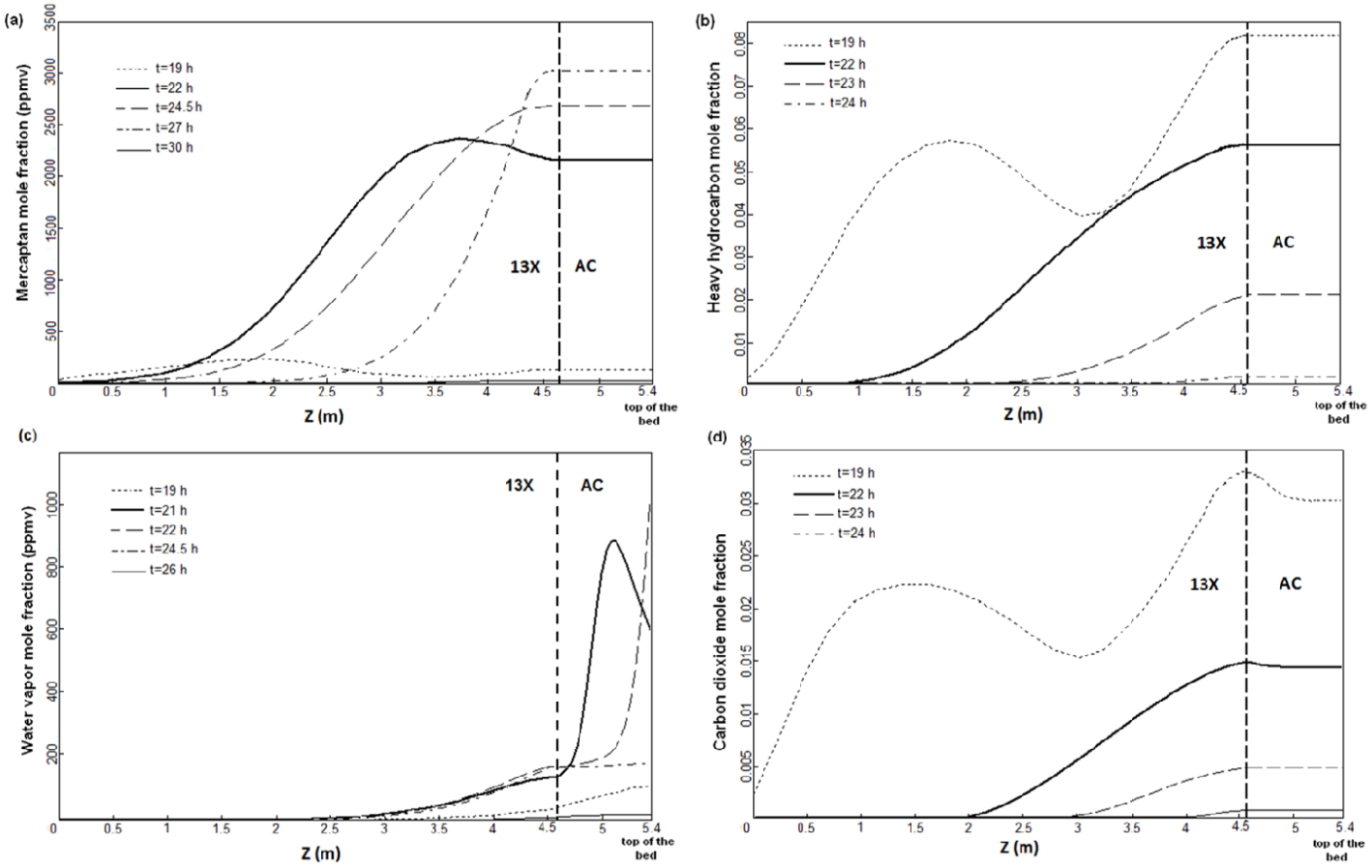

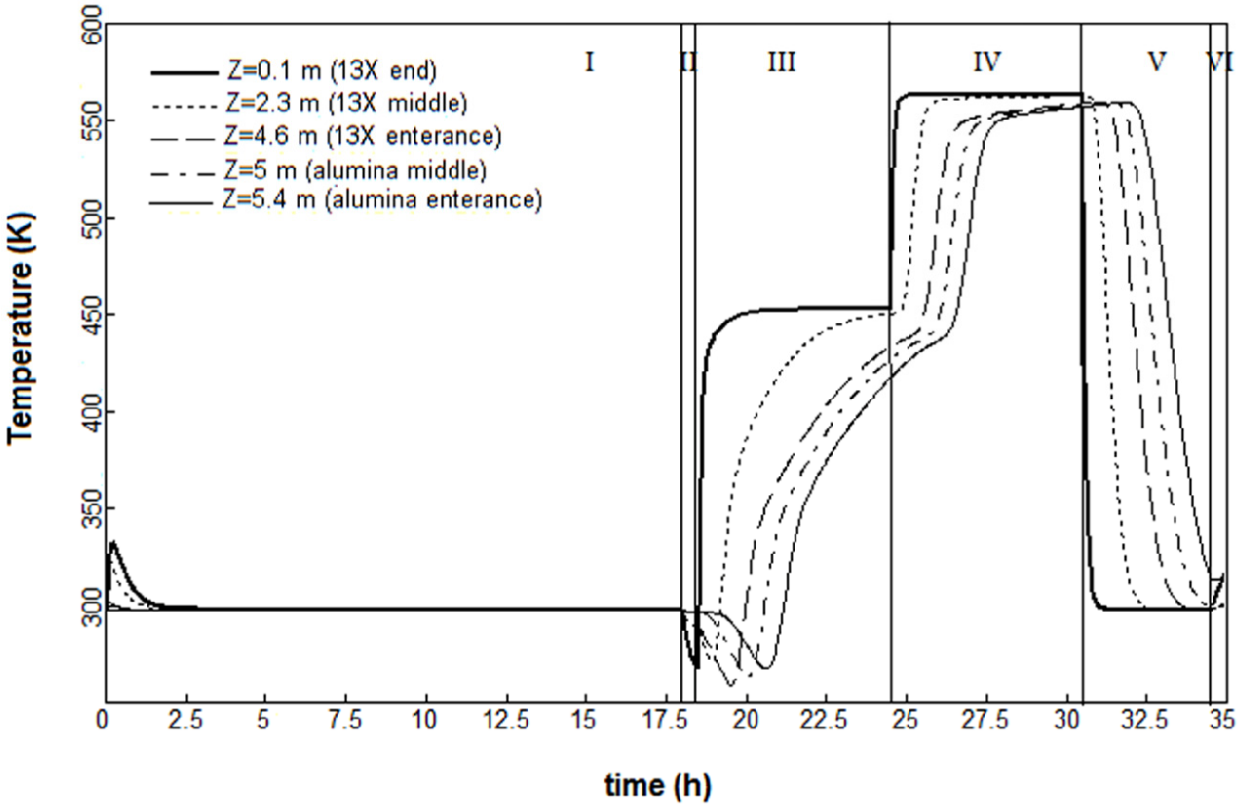

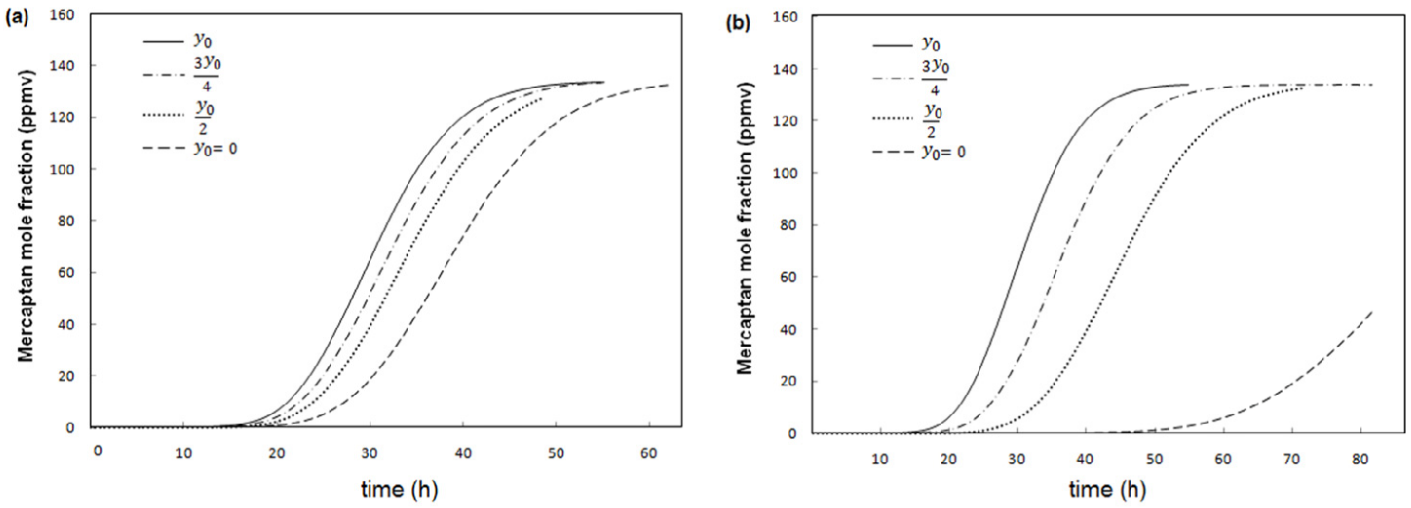

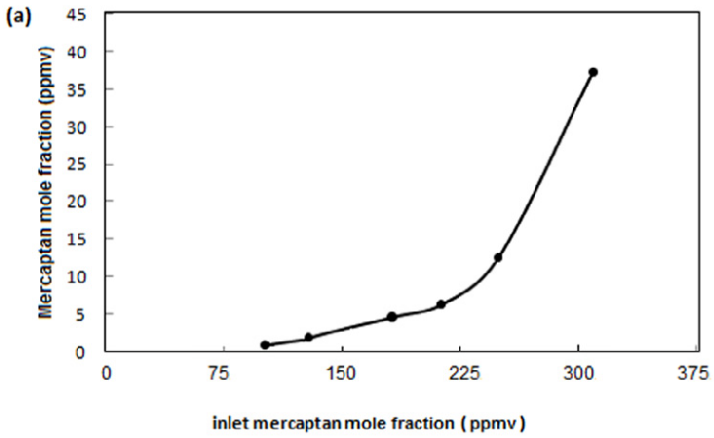

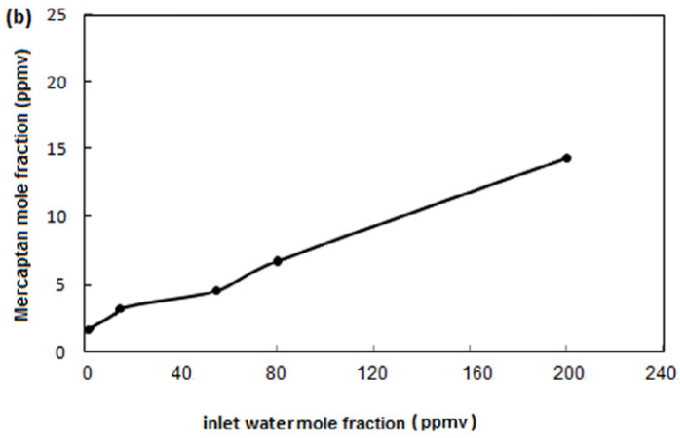

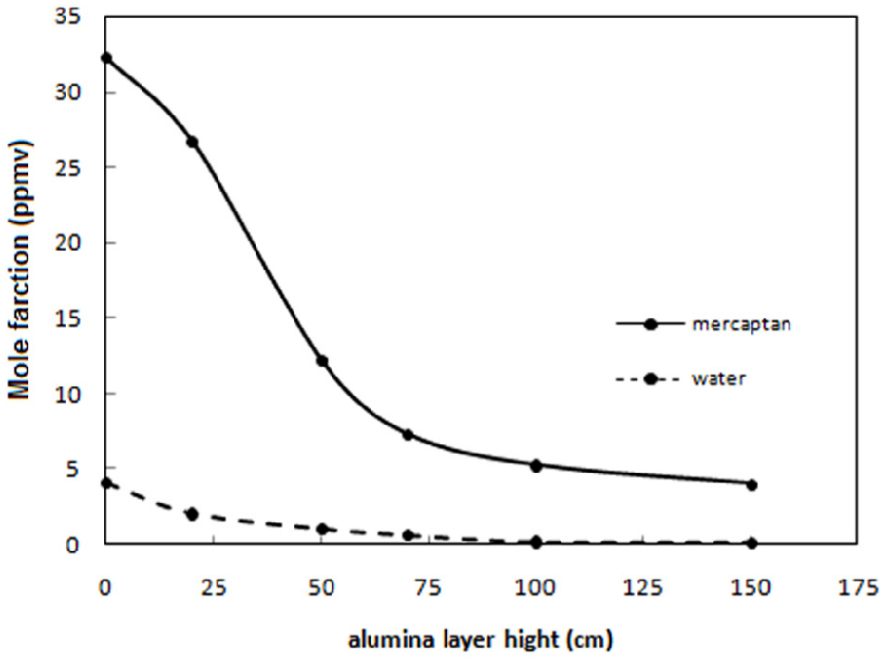

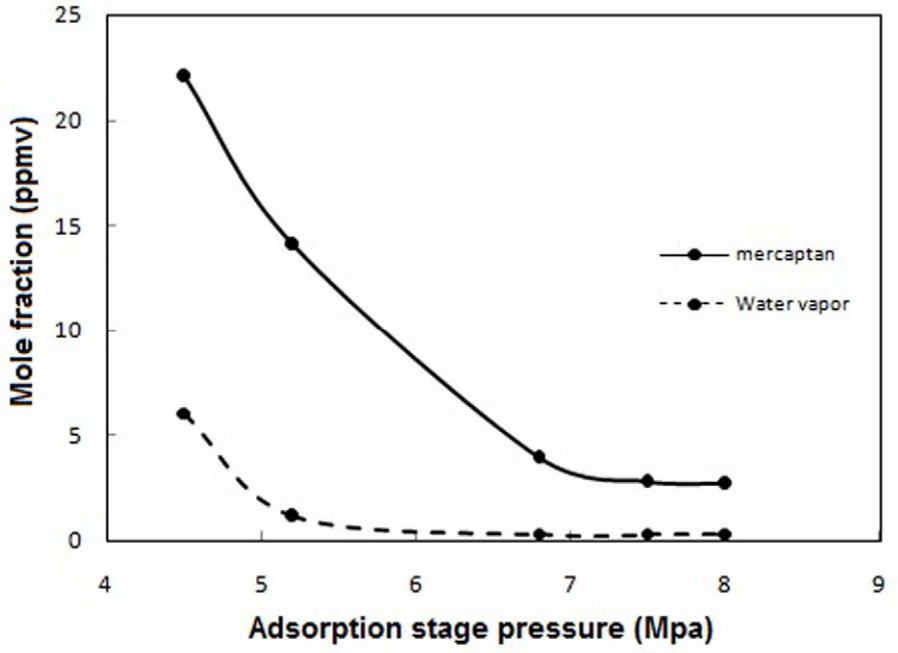

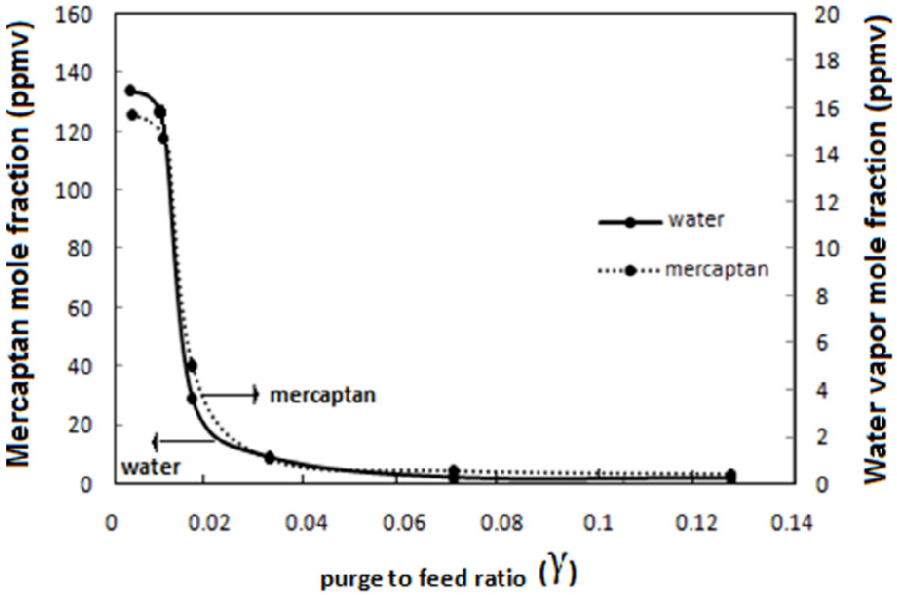

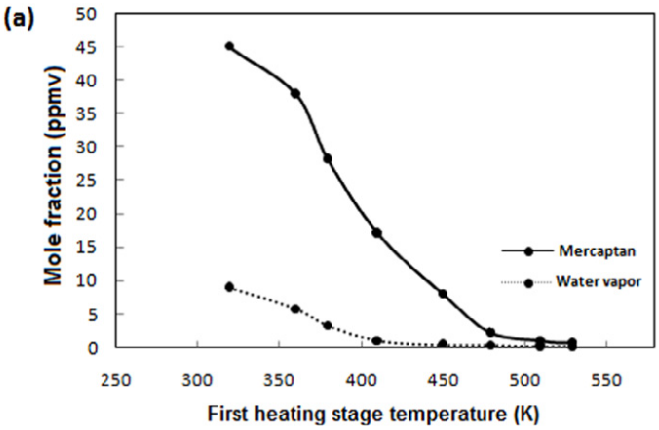

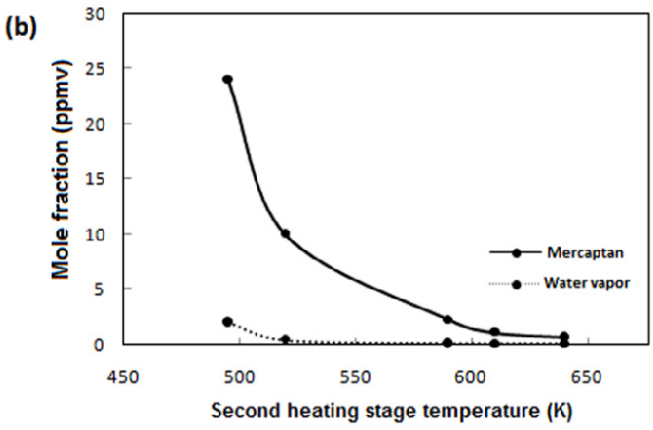

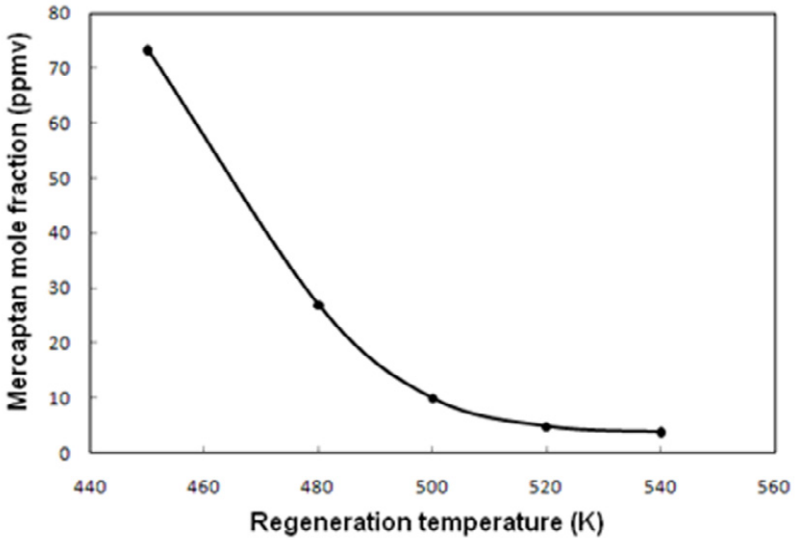

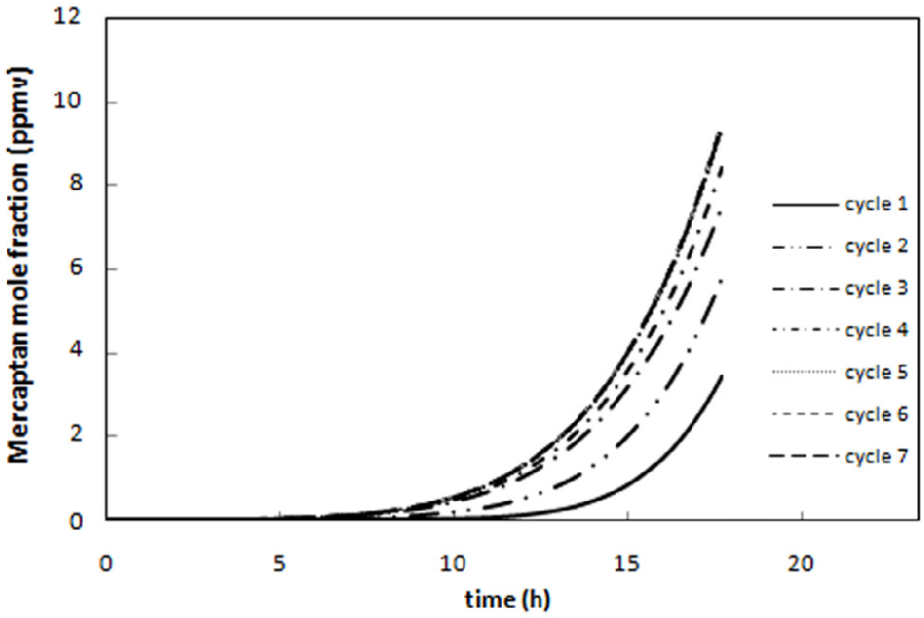

Graphical Abstract

Simple diagram of the sequential TPSA process description.

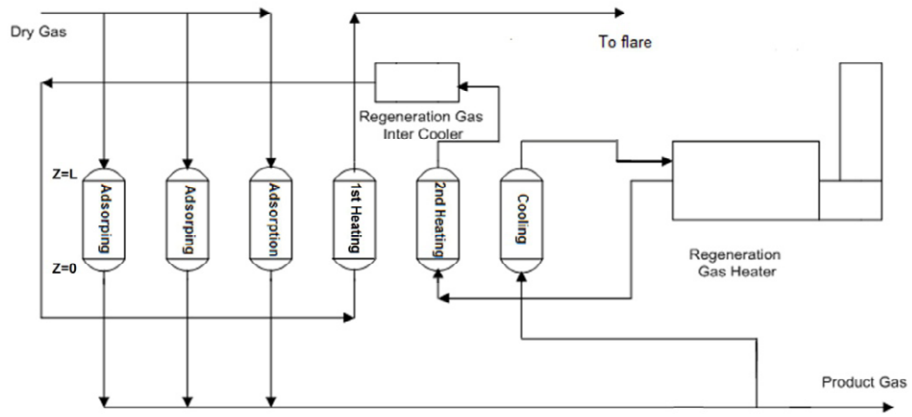

Operating bed pressure (a); and temperature (b); with elapsed time

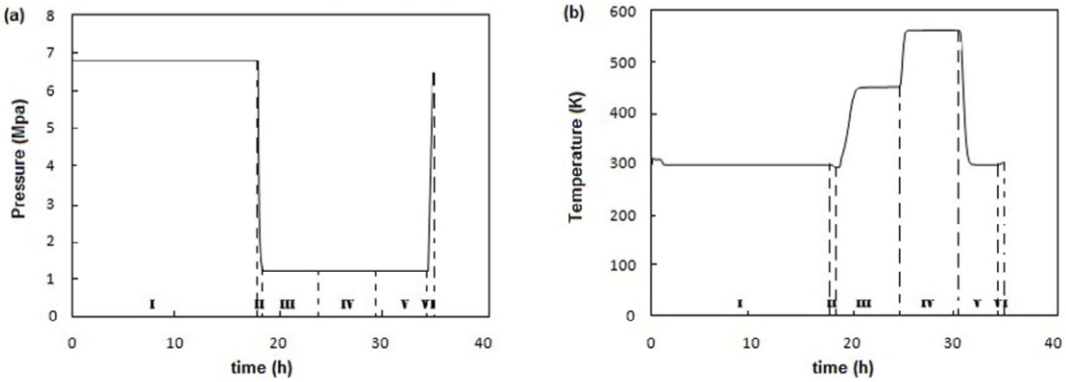

Good agreement between simulated results and operational

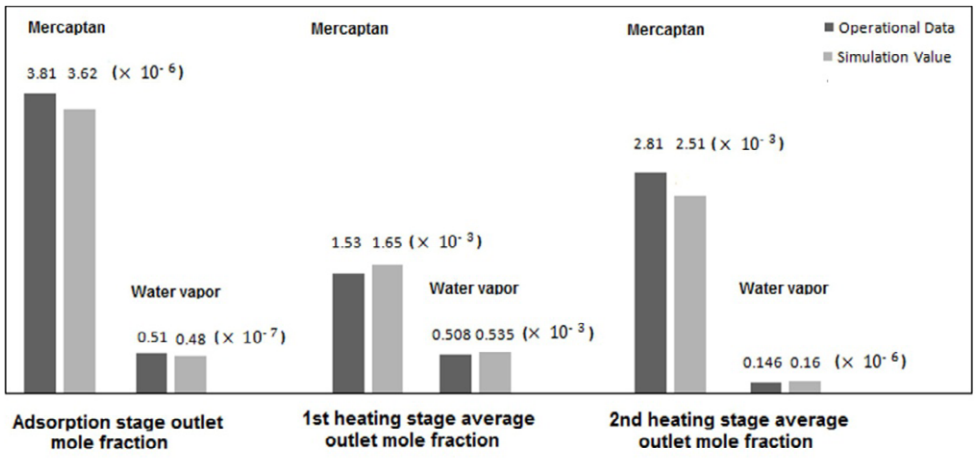

Highlights

1. Modeling and Simulation of Industrial cyclic Pressure-Temperature Swing Adsorption unit
2. Natural gas feed was considered as a mixture of CH4, CO2, H2O, C3+ and light mercaptanes
3. The influence of operational parameters was investigated on the natural gas purity and energy consumption